JOURNAL OF QUATERNARY SCIENCE (2016) **9999**(9999) 1–23 ISSN 0267-8179. DOI: 10.1002/jqs.2905

Chronology and processes of late Quaternary hillslope sedimentation in the eastern South Island, New Zealand

Q1 JOSH BORELLA,[1]* MARK QUIGLEY,[2] REZA SOHBATI,[3,4] PETER ALMOND,[5] DARREN GRAVLEY[1] and ANDREW MURRAY[4] Q1
[1]Department of Geological Sciences, University of Canterbury, New Zealand
[2]School of Earth Sciences, The University of Melbourne, Victoria 3010, Australia
[3]Centre for Nuclear Technologies, Technical University of Denmark, DTU-Nutech, DTU Risø Campus, DK-4000, Roskilde, Denmark
[4]Nordic Laboratory for Luminescence Dating. Department of Geoscience, Aarhus University, DTU Risø Campus, DK-4000, Roskilde, Denmark
[5]Department of Soil and Physical Sciences, Lincoln University, New Zealand

Received 12 March 2016; Revised 7 September 2016; Accepted 8 September 2016

ABSTRACT: Optical and radiocarbon dating of loessic hillslope sediments in New Zealand's South Island is used to constrain the timing of prehistoric rockfalls and associated seismic events, and quantify spatial and temporal patterns of hillslope sedimentation including responses to seismic and anthropogenic forcing. Exploratory trenches adjacent to prehistoric boulders enable stratigraphic analysis of loess and loess-colluvium pre- and post-dating boulder emplacement, respectively. Luminescence ages from loessic sediments constrain the timing of boulder emplacement to between ~3.0 and ~12.5 ka, well before the arrival of Polynesians (ca. AD 1280) and Europeans (ca. AD 1800) in New Zealand, and suggest loess accumulation was continuing at the study site until 12–13 ka. Large (>5 m^3) prehistoric rockfall boulders preserve an important record of Holocene hillslope sedimentation by creating local traps (i.e. accommodation space) for sediment aggradation (i.e. colluvial wedges) and upbuilding soil formation. Sediment accumulation rates increased considerably (>~10 factor increase) following human arrival and associated anthropogenic burning of hillslope vegetation. Our study presents new numerical ages to place the evolution of loess-mantled hillslopes in New Zealand's South Island into a longer temporal framework and highlights the roles of earthquakes and humans on hillslope surface process.

Introduction

Hillslope sediments provide a potentially valuable archive of contemporary and paleo-landscape processes (e.g. Fuchs and Lang, 2009; Fuchs *et al.*, 2010). Dating of slope sediments has been extensively used for understanding landscape response to local and global climate change (e.g. Hanson *et al.*, 2004), anthropogenic influences on hillslope sediment erosion and accumulation (e.g. Roering *et al.*, 2002, 2004; Fuchs *et al.*, 2004, 2010; Almond *et al.*, 2008; Hughes *et al.*, 2010; Borella *et al.*, 2016), and tectonic activity (e.g. Fattahi *et al.*, 2006). Additionally, hillslope sediment chronologies have been used to determine the timing of mass wasting events, such as landslides and rockfalls (Becker and Davenport, 2003; Matmon *et al.*, 2005; Kanari, 2008; Chapot *et al.*, 2012; Mackey and Quigley, 2014; Rinat *et al.*, 2014).

Various methods have been used to date hillslope sediments (e.g. Jibson, 1996; Lang *et al.*, 1999), including radiocarbon dating (^{14}C) (e.g. Stout, 1969; Becker and Davenport, 2003; Bertolini, 2007), lichenometry (e.g. Bull *et al.*, 1994; Luckman and Fiske, 1995; André, 1997; McCarroll *et al.*, 2001), dendrochronology (e.g. Stoffel, 2006) and optically stimulated luminescence (OSL) dating (e.g. Matmon *et al.*, 2005; Balescu *et al.*, 2007; Chapot *et al.*, 2012). Cosmogenic nuclide (CN) surface exposure dating has also been implemented to determine the emplacement time for boulders entrenched within hillslope sediments (e.g. Cordes *et al.*, 2013; Mackey and Quigley, 2014; Rinat *et al.*, 2014; Stock *et al.*, 2014a,b) and estimate production rates and residence times of colluvial hillslope soils (e.g. Heimsath *et al.*, 2002). Increased confidence in hillslope sediment chronologies can be obtained by combining OSL, ^{14}C and CN (e.g. Lang and Wagner, 1996; Rinat *et al.*, 2014) dating methods.

New Zealand's South Island provides a variety of important opportunities for investigating the spatiotemporal behavior of surface processes and their response to climatic, seismic and anthropogenic forcing (Glade, 2003; Woodward and Shulmeister, 2005; Almond *et al.*, 2008; Hughes *et al.*, 2010; Rowan *et al.*, 2012; Fuller *et al.*, 2015). Prehistoric rockfall boulders at Rapaki (NZ) preserve an important record of Holocene hillslope soil transport. In this paper we examine the influence of large (>~5 m^3) rockfall boulders on local hillslope morphology and soil evolution. We perform detailed analysis (e.g. stratigraphic logging, grain-size analysis, sediment bulk density) and OSL and ^{14}C dating of loessic hillslope sediments to constrain the timing of prehistoric rockfall and associated earthquakes, and quantify the spatial and temporal patterns of hillslope sedimentation including responses to seismic and human activity.

In combination with Sohbati *et al.* (2016) we present the first successful (i.e. reliable luminescence ages) optical dating of coarse-grained (i.e. >11 μm) loess and loess-colluvium hillslope sediments in New Zealand using the SAR protocol for quartz and pIRIR$_{290}$ protocol for K-rich feldspar. Our numerical (luminescence and radiocarbon) ages provide a uniquely detailed chronology for understanding the evolution of loess-mantled hillslopes in New Zealand's South Island through the late Pleistocene and Holocene epochs. This study highlights the roles of earthquakes and humans on hillslope surface process, and demonstrates the value of

*Correspondence: J. Borella, as above.
E-mail: josh.borella@pg.canterbury.ac.nz

rockfall-emplaced boulders on hillslopes for creating archives of past hillslope responses.

Geologic setting

Geology of Banks Peninsula and the Port Hills

Banks Peninsula (Fig. 1) comprises three main volcanoes active between ~11.0 and 5.8 Ma (Hampton and Cole, 2009). The study site is located within the dissected Lyttelton Volcanic complex (~11.0–9.7 Ma) on the western side of Banks Peninsula (Fig. 1). Bedrock of the Lyttelton Volcanic complex is composed of subaerial basaltic and trachytic lava flows interlayered with ash and/or paleosol packages (Forsyth *et al.*, 2008; Hampton and Cole, 2009). The volcanic rocks are mantled by four principal regolith materials: loess, loess-colluvium, mixed loess-volcanic colluvium and volcanic colluvium, as defined by Bell and Trangmar (1987).

The initiation and timing of regionally sourced (Southern Alps and Canterbury Plains, see Fig. 1) loess accumulation on Banks Peninsula has been the subject of previous studies at multiple locations (e.g. Griffiths, 1973; Ives, 1973). Results from Almond *et al.* (2007b) indicate the last major phase of loess accumulation on the lower flanks of Banks Peninsula in Canterbury began before *ca.* 35k cal a BP. In South Canterbury (Timaru) and based upon radiocarbon ages presented by Runge *et al.* (1973), Tonkin *et al.* (1974) proposed that loess accumulation ceased around ~10 000 cal a BP, with the last major accumulation phase between 9900 and 11 800 cal a BP (Goh *et al.*, 1977, 1978). On Banks Peninsula, Griffiths (1973) reports an age of 17 450 ± 2070 cal a BP (radiocarbon age from humic acid) from the top of the first paleosol at Barrys Bay. However, Goh *et al.* (1977, 1978) demonstrated that these ages were underestimates due to contamination. At Ahuriri Quarry, Banks Peninsula, Almond *et al.* (2007b) report a carbonate radiocarbon age range of 9927–10 235 cal a BP for youngest loess sediments, but warn that pedogenic carbonate is a post-depositional precipitate, and thus ages derived from carbonate-containing loess must be considered minimum loess ages. Several luminescence ages of *ca.* 17 ka are generated within the upper loess unit (see Almond *et al.*, 2007b – Unit 1a) but also show inconsistency with the position and accepted age of ~25.4k cal a BP for Kawakawa/Oruanui tephra (Vandergoes *et al.*, 2013), bringing into question their reliability.

Almond *et al.* (2008) investigated hillslope response at Ahuriri Quarry on the western flank of Banks Peninsula and concluded that most erosion occurred in the Holocene after the primary loess accumulation phase (~35–17 ka), consistent with an increase in soil flux rates with Holocene climate amelioration and recolonization by forest. Their results suggest a complex interaction between climate, vegetation, land management and soil transport on soil-mantled hillslopes. Bell and Trangmar (1987) present an in-depth study of regolith materials and erosion processes for slopes in the Port Hills of Banks Peninsula (western side) but no temporal constraint (i.e. absolute dating) is provided for colluvial sediments, emplacement of prehistoric rockfall or removal of slope vegetation. The general effects of meteorological phenomena on slope process are considered but the impacts of earthquakes and humans on hillslope evolution were not examined.

Paleoclimate and paleovegetation of Banks Peninsula

The understanding of past climate and vegetation in Banks Peninsula is increasing (e.g. Wilson, 1993; Shulmeister *et al.*, 1999; Soons *et al.*, 2002), but establishing temporal bounds for local and regional climate/vegetation changes remains a primary challenge. Shulmeister *et al.* (1999) employed a multi-technique approach (e.g. radiocarbon dating, thermoluminescence) supported by proxy data (diatoms, phytoliths, pollen) to show that the pre-European flora of Banks Peninsula was dominated by mixed podocarp broadleaf forests during interglacial periods and replaced by tall shrubland of mixed montane and coastal affinities during cooler glacial phases. Pollen diagrams from South Island consistently show a transition from grassland to shrubland (during the Lateglacial) to forest (i.e. podocarp/hardwood)

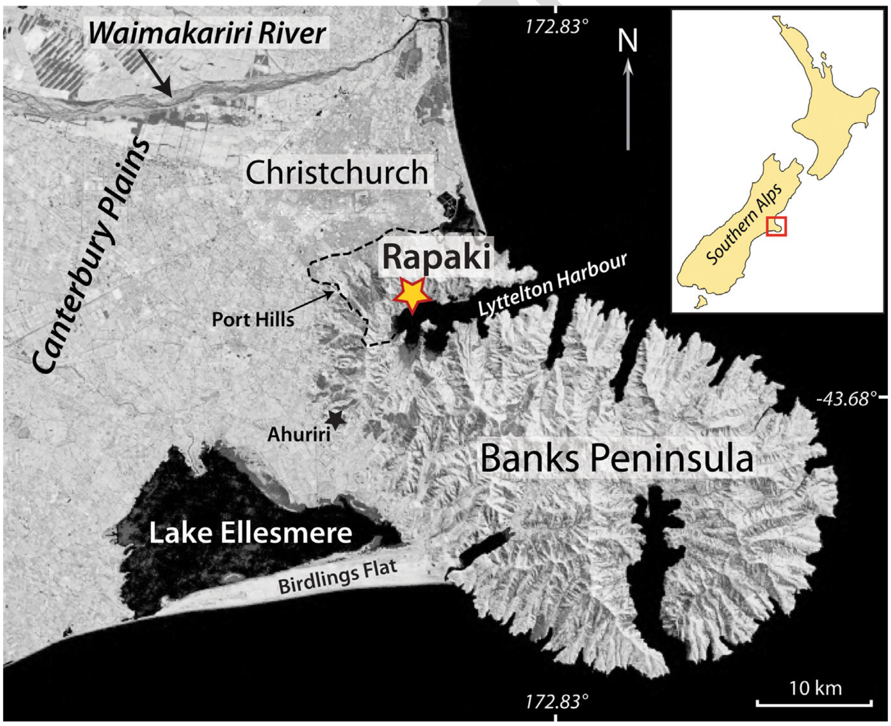

Figure 1. Location map showing Rapaki study site and surrounding Port Hills and greater Banks Peninsula.

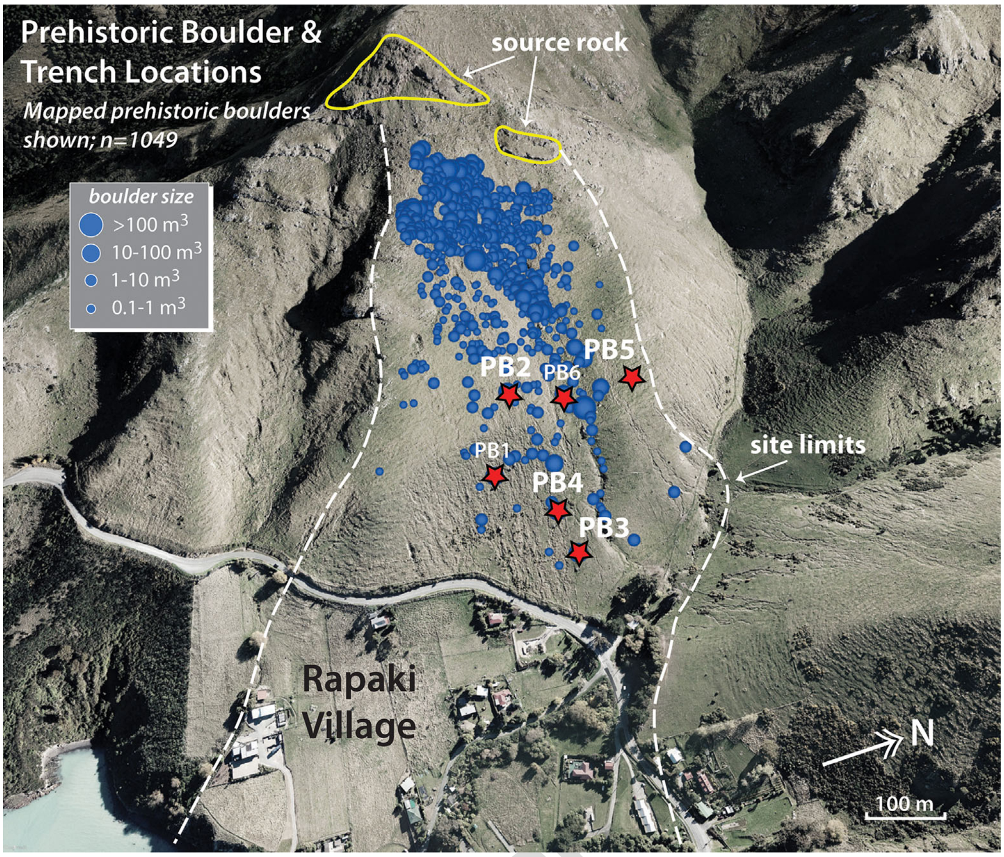

Figure 2. Rapaki study slope with prehistoric boulder and trench locations. Detailed logging was performed for PB2, PB3, PB4 and PB5 trenches. Mapped prehistoric boulders reflect boulder volume $\geq 0.1\ m^3$.

around the Holocene boundary (Shulmeister *et al.*, 1999; Woodward and Shulmeister, 2005). Native forest in Banks Peninsula was modified by two separate phases of human activity, beginning with the Polynesians (Maori) 700–800 cal a BP and continuing with the Europeans, who settled the area approximately 150 years ago (McGlone, 1989; Harding, 2003; McWethy *et al.*, 2010). By 1900, Europeans had removed >98% of the indigenous forest (Harding, 2003; Wilson, 2008, 2013), leaving slopes vulnerable to accelerated erosion and mass wasting (Glade, 2003). Borella *et al.* (2016) demonstrate that anthropogenic deforestation in Banks Peninsula has increased the rockfall hazard by enabling modern boulders to travel further downslope than their prehistoric predecessors.

Rapaki Study Site

The Rapaki study site (Figs 1–4) occupies the northern half of the south-eastern slope of Mount Rapaki (Te Poho o Tamatea), situated above Rapaki village in Banks Peninsula.

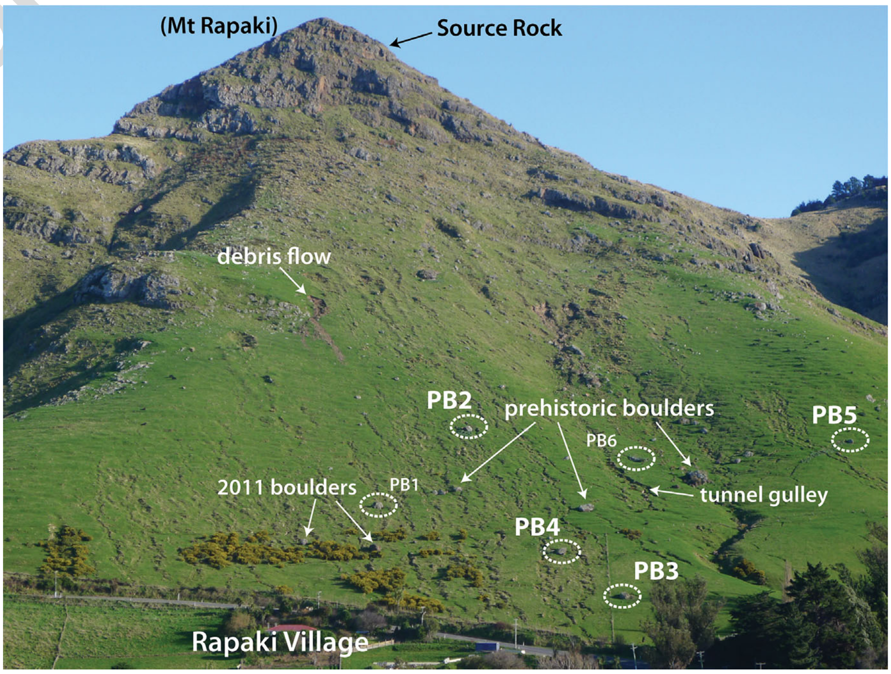

Figure 3. Prehistoric and modern (2011) boulders at the Rapaki study site. Prehistoric boulders are distinguishable from modern rockfall deposits because they are partially embedded in hillslope colluvium and are visible in pre-Canterbury earthquake sequence imagery. Surficial landslides (e.g. debris and mud flow) and extensive tunnel gulley formation and erosion are extensive on the modern deforested landscape. Locations for studied prehistoric boulders PB1–PB6 are shown. Detailed trench logging was performed for PB2–PB5.

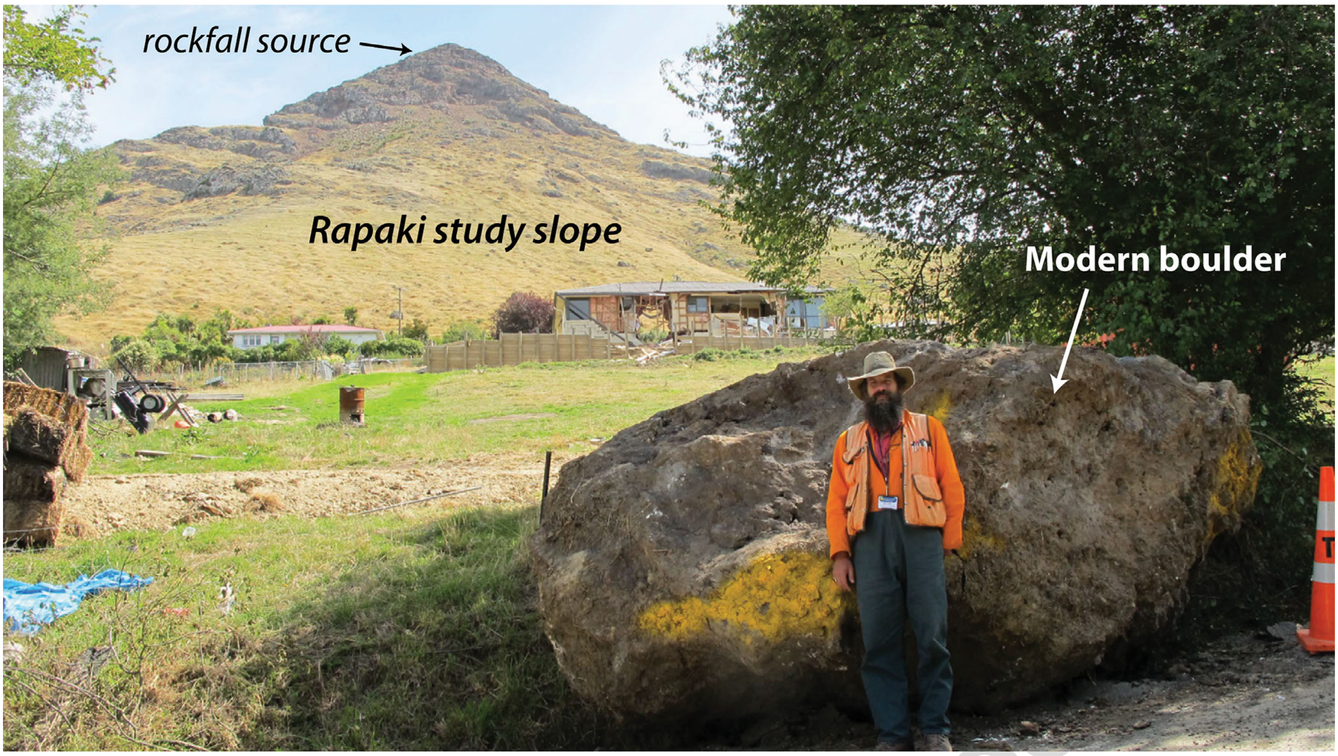

Figure 4. Large modern boulder (~28 m^3) detached from Mount Rapaki and emplaced in the Rapaki village during the 22 February 2011 earthquake. The boulder traveled through the center of the residential home located in background (center). Photo courtesy of D. J. A. Barrell, GNS Science.

The hillslope is slightly concave in profile with a total area of approximately 0.21 km^2, and bounded in its upper part by steep to subvertical bedrock cliffs comprising distinct sub-horizontal packages of coherent, vertically to irregularly jointed basaltic lava flows separated by indurated volcanic breccias. The bedrock cliffs are ~60 m tall and ~300 m wide. A ~23° sloping grassy hillslope underlain by loess, loess and volcanic (i.e. sourced from volcanic bedrock) colluvium, and overlying prehistoric and modern rockfall boulders is subjacent to the bedrock cliffs. Rapaki village lies at the hillslope base, from approximately 70 m (asl) to sea level. The removal of slope vegetation (i.e. native forest) has left the existing hillslope vulnerable to erosion, such as surficial landsliding (i.e. debris and mudflow) and tunnel gulley erosion (Fig. 3).

Rockfall deposits sourced from the upslope bedrock cliffs are a prominent surface feature at Rapaki (Fig. 3). More than 650 individual modern (2011) boulders ranging in diameter from <15 cm to >3 m were dislodged from the bedrock source cliffs near the top of Mount Rapaki on 22 February and 13 June 2011 Canterbury earthquakes (Heron *et al.*, 2014; Mackey and Quigley, 2014; Massey *et al.*, 2014; Borella *et al.*, 2016). Twenty-six of these boulders, ranging in volume from ~0.25 to ~28.0 m^3, reached Rapaki village. Individual boulders (Fig. 1D) travelled up to 770 ± 15 m downslope from the source cliff. Prehistoric fallen boulders are found interspersed with modern rockfall and are more abundant than their 2011 counterparts at Rapaki, where we mapped and characterized 1543 rocks ranging in volume from 0.001 to >100 m^3 (Borella *et al.*, 2016) (Figs 2 and 3). Mackey and Quigley (2014) used cosmogenic ^{3}He surface-exposure dating on 19 paleo-boulder surfaces to estimate the emplacement time of prehistoric rockfall at Rapaki. Rockfall was attributed to a strong proximal earthquake at 6–8 ka, with another potential prehistoric rockfall event occurring 13–14 ka.

Methods

Stratigraphic analysis and sampling

Prehistoric boulders and adjacent trench locations for stratigraphic analysis and sampling were selected based upon the following criteria. The prehistoric boulder should (i) be large enough (>5.0 m^3) to ensure subaerial exposure and sufficiently buried to ensure post-emplacement stability; (ii) be located away from drainage valleys to limit post-emplacement mobility and sediment depositional complexities; (iii) have a thick colluvial wedge developed upslope with no evidence of pervasive late-stage tunnel gulley erosion or anthropogenic and livestock modification; and (iv) have a surface exposure age (Mackey and Quigley, 2014) so that cross-validation between luminescence and CN surface exposure dating methods could be performed. Four prehistoric boulders (PB23–PB5) were chosen for detailed investigation (Figs 2 and 3; Supplementary Table S1) and two (Figs S1 and 2 – PB1 and PB6) for more cursory description.

Dating methods

We use luminescence and radiocarbon dating techniques to constrain the age of hillslope sediments and CN concentrations for prehistoric boulders (Mackey and Quigley, 2014). Luminescence dating provides a numerical age estimate of the last exposure to daylight of minerals such as quartz and feldspar (Aitken, 1998), while radiocarbon dating estimates the time elapsed since the death of an animal or plant. We use charcoal ages as a proxy for timing of sediment deposition, assuming charcoal originated from young wood, and that erosion, transport and deposition of the charcoal-containing sediment occurred shortly after burning. Cosmogenic exposure ages estimate the length of time that a rock surface has been subaerially exposed, and rely on a simple exposure history for their accuracy (Heyman *et al.*, 2011).

Luminescence dating

Thirteen samples were collected for luminescence dating in (i) loess deposits underlying the prehistoric boulders and (ii) loess-colluvium accumulated upslope (i.e. colluvial wedge) of the boulders after emplacement on the hillside (Sohbati *et al.*, 2016). Sampling involved pushing 5-cm-diameter stainless-steel tubes (15 cm in length) into cleaned sections of the trench walls. To constrain emplacement timing for each of the prehistoric boulders, samples were collected within sediments lying directly below (maximum age) and above (minimum age) the geomorphic surface the boulder rested on.

Luminescence samples were analysed at The Nordic Centre for Luminescence Research in Roskilde, Denmark. Luminescence sample preparation and analytical details are provided in Sohbati *et al.* (2016). Optical ages are labeled on corresponding trench logs (Figs 5C, 6C, 7C, 9C and 10B) and presented in Table 1.

Radiocarbon dating

Radiocarbon assays were performed on four individual pieces of charcoal to constrain the depositional age of the post-boulder emplacement colluvial sediments. Charcoal was retrieved near the base of the youngest colluvial sediments (LC_R) in PB3 and PB4. Charcoal samples ranging between 70 and 500 mg were submitted to the Rafter Radiocarbon Laboratory in Wellington, New Zealand, for accelerator mass spectrometry (AMS) radiocarbon analysis. Ages were calibrated using the Southern Hemisphere calibration curve (SHCal13; Hogg *et al.*, 2013)[Q2]. We report both 2σ and 1σ calendar-calibrated ^{14}C age ranges in the text and both calibrated and conventional radiocarbon ages in Table 2 (see Figs S3–6).

Results

Trench stratigraphy

In situ loess

Putative *in situ* loess beneath the boulders comprises the oldest sediment in each of the trenches (Figs 5–10). It consists of a light yellowish brown to light olive brown, massive, hard and dry silt to fine sandy loam and contains essentially no (≤0.2%) sediment derived from the proximal volcanic source rock (i.e. basalt) (Table 3a–d; Table S2). The loess exhibits characteristic gammate structure with grey fissures/veins and desiccation cracks with infilling translocated clay, as pedogenic carbonate rhizomorphs.

Preboulder Soil Stratigraphic Unit (PB-SSU)

The PB-SSU is a buried soil formed in ~13–44 cm of colluvium above the *in situ* loess and below the boulders. The PB-SSU comprises a morphological B horizon that probably includes a former A horizon, characterized by a light olive brown to grayish brown to light yellowish brown, massive to very poorly layered, hard, dry to occasionally damp, silt loam with minor (≤1%) gravel, pebble and cobble-sized basalt clasts (Table 3a–d; Table S2).

Development of PB-SSU is most advanced within PB2, PB4 and PB5 (maximum thickness ~44 cm) trenches, and displays abundant mottling, clay coatings/worm casts, millimetre-scale voids (burrows, dissolved roots) and calcite-filled desiccation cracks (Table 3a–d; Table S2). PB-SSU thickness is generally consistent adjacent to and beneath the boulders, with the exception of PB2, where it thins beneath the boulder (perhaps due to compaction from the overlying boulder).

An irregular disconformity is observed at the top of the PB-SSU within each of the trenches. This surface marks the boundary between sediments that pre-date boulder emplacement (i.e. loess and colluvium) and those accumulating after boulder deposition (i.e. colluvium only).

Loess colluvium (LC)

A 50–130-cm-thick wedge of loess colluvium has accumulated upslope of PB2–PB5 and must post-date these boulders. We define this lithostratigraphic unit as LC (Figs 5–10). Differences in texture, density, color and relative moisture content were used to distinguish between the older loess (including PB-SSU) sediments and younger loess colluvium (LC) deposits (Table 3a–d). LC consists of a brown to dark grayish brown, massive to poorly layered, soft to firm, damp to semi-moist, silt loam (Table 3a–d). Gravel-sized clasts (3–6 mm in diameter) are commonly encountered within the predominantly silty matrix. We observed a marked increase in volcanic-derived (basaltic) material within LC (Table S2), ranging in size from medium- to coarse-grained sand and gravel to pebble- and small boulder-sized volcanic rocks. Maximum abundance of volcanic clasts is ~17%. LC contains abundant small rootlets and pervasive yellowish brown to brownish yellow mottling.

Loess Colluvium – Recent (LC_R)

LC_R post-dates boulder emplacement and accumulation of LC. It is observable within the PB3 trench and possibly the PB4 trench (Figs 3B,C and 4B,C), and represents the most recent phase of colluviation. In PB3, LC_R comprises a grayish brown to very dark gray, poorly to moderately layered, soft, dry to slightly damp, silt loam with minor gravel (Table 3b,c). Q2
Charcoal was observed within the lower 30 cm and within sediment deposited around the sides of PB3 (at base). Radiocarbon dates for the charcoal fragments are presented in Table 2 and Figs S3–5. At approximately 52 cm depth from the ground surface, charcoal is mixed with small fragments (mm to cm scale) of orange to reddish orange baked volcanic rock or brick/pottery, the latter indicating possible later European burning and suggesting that colluvium above this level occurred during European settlement. For PB4, we propose the upper ~35–50 cm of LC may be roughly time equivalent to the LC_R sediments observed in PB3. A 1- to 2-mm fragment of charcoal has been logged at a depth of ~33 cm from the existing ground surface. Radiocarbon dating of the charcoal fragment has been performed and results are presented in Table 2 (also see Fig. S6).

Infill events

Infill events post-date boulder emplacement and deposition of adjacent LC and, in some cases, LC_R colluvial sediments. Two separate infill events (IF-1 and IF-2) were observed at the boundary between the PB2 boulder and loess colluvial wedge sediments (Fig. 5C and Table 3a). We propose that space created at the back of PB2 for infilling may have resulted from several processes including (i) minor shifting of the boulder during earthquake-induced shaking, (ii) desiccation and subsequent contraction of sediment adjacent to PB2, and/or (iii) erosion of preexisting sediment at the boulder–sediment boundary. A single infill (IF-1) event is observed adjacent to PB4 (Fig. 8) and consists of dark gray sandy silt (Table 3c). The sediment appears recent and has filled in space created adjacent (and partially beneath) to the upslope side of the boulder. PB4 infill is similar in character (i.e. texture, composition) to IF-2 observed in PB2 trench sediments (Fig. 5B,C). PB4 records only a single infill event and may reflect a higher *in situ* stability or younger boulder

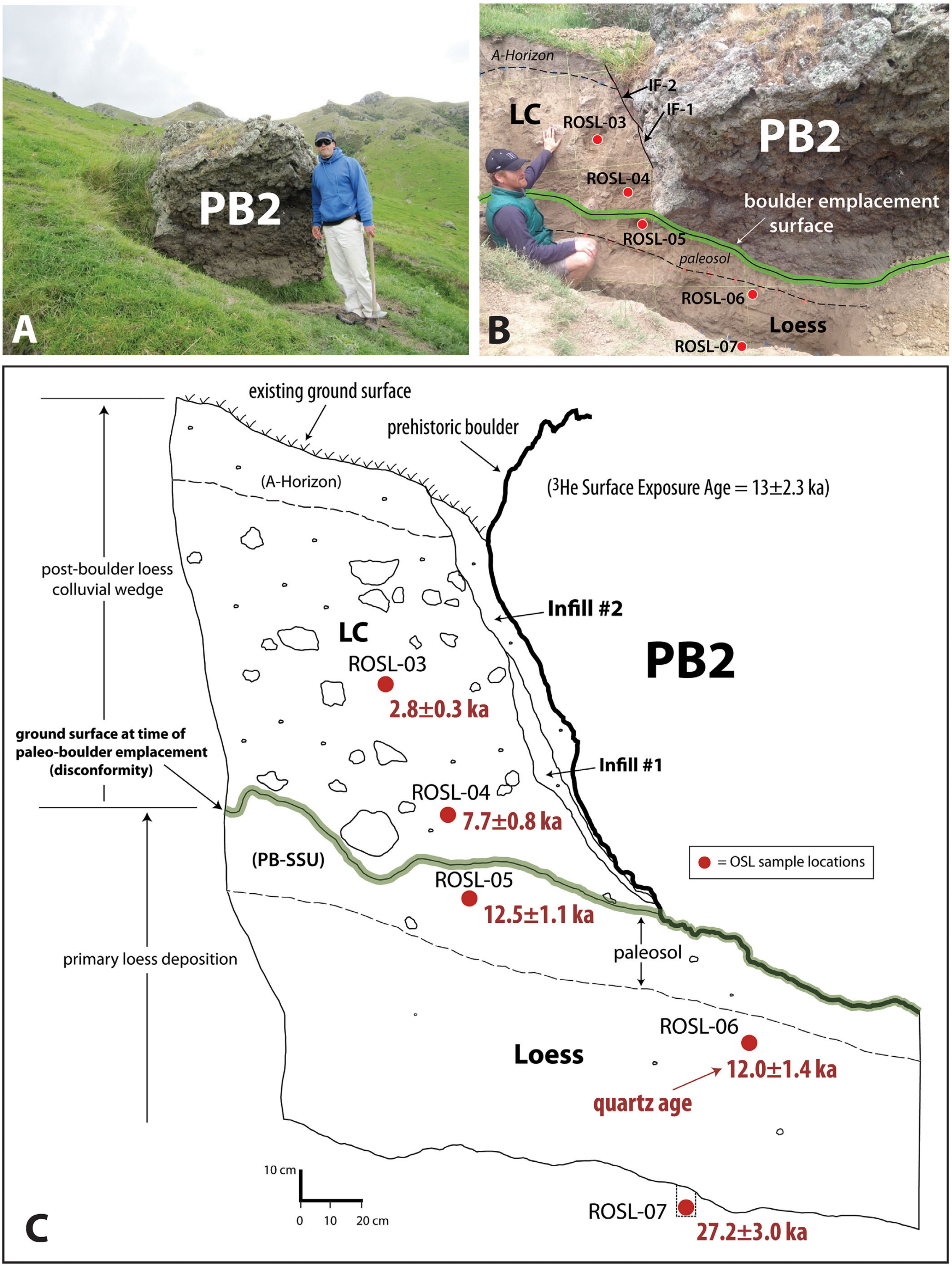

Figure 5. Prehistoric Boulder #2. (A) Photo of PB2 and surrounding hillslope sediment before exploratory trenching. (B) Photo of PB2 with pre-boulder (loess) and post-boulder (loess-colluvium) emplacement hillslope sediments exposed. (C) Detailed stratigraphic log of PB2 and surrounding loess and loess-colluvium (LC) sediments. PB-SSU (Preboulder Soil Stratigraphic Unit) is present at top of loess. OSL sample locations and quartz luminescence ages are shown. Mackey and Quigley (2014) ^{3}He CN surface exposure age for PB2 is shown.

Table 1. Summary of Rapaki (NZ) sample name, boulder/trench location, burial depth, quartz OSL and K-feldspar $pIRIR_{290}$ ages (Modified from).

Sample name	Boulder/trench location	Sample depth (cm)	Quartz OSL age (ka, mean ± SE)	K-feldspar $pIRIR_{290}$ age (ka, mean ± SE)
ROSL-02	PB1	247	29.3 ± 2.5	28.5 ± 1.6
ROSL-03	PB2	70	2.8 ± 0.3	2.46 ± 0.15
ROSL-04	PB2	99	7.7 ± 0.8	6.9 ± 0.4
ROSL-05	PB2	116	12.5 ± 1.1	10.8 ± 0.6
ROSL-06	PB2	87	12.0 ± 1.4	10.2 ± 0.6
ROSL-07	PB2	171	27.2 ± 3.0	21.8 ± 1.4
ROSL-08	PB3	81	2.9 ± 0.3	2.6 ± 0.2
ROSL-09	PB3	170	5.8 ± 0.5	6.5 ± 0.4
ROSL-10	PB4	93	4.2 ± 0.4	3.8 ± 0.2
ROSL-11	PB4	120	10.3 ± 1.0	10.4 ± 0.7
ROSL-12	PB4	131	13.4 ± 1.2	12.7 ± 0.7
ROSL-13	PB5	31	1.7 ± 0.2	1.94 ± 0.14
ROSL-14	PB5	110	10.2 ± 0.8	12.6 ± 0.8

emplacement age compared with PB2. No late infilling events are observed at the boundary between the loess colluvial wedge sediments and upslope side of PB3 and PB4.

OSL and radiocarbon chronology

The luminescence samples were dated using the single-aliquot regenerative-dose (SAR) protocol (Murray and Wintle, 2003) for blue-light-stimulated luminescence of quartz (quartz OSL) and post-infrared-stimulated luminescence (IRSL) of potassium-rich feldspar (K-rich feldspar $pIRIR_{290}$) (Buylaert *et al.*, 2012) grains (i.e. 40–63 µm). Details of luminescence characteristics, equivalent doses, dose rates and ages are given in Sohbati *et al.* (2016). Despite the excellent agreement between the quartz OSL and K-feldspar $pIRIR_{290}$ ages, which assures the overall reliability of the optical ages (Sohbati *et al.*, 2016), we base our geologic interpretation on quartz OSL ages because the quartz signal does not suffer from the complications usually associated with the K-feldspar signals such as stability and complete resetting in nature (Sohbati *et al.*, 2016).

PB2

The OSL age for ROSL-07 indicates loess accumulation 27.2 ± 3.0 ka and agrees well with the quartz OSL age from ROSL-02 (29.3 ± 2.5 ka) (Table 1; Fig. S1). The luminescence age for ROSL-06 suggests that loess accumulation at Rapaki may have occurred as late as 12.0 ± 1.4 ka. The OSL age within the PB-SSU (ROSL-05) indicates a statistically similar age of 12.5 ± 1.1 ka (Fig. 2C), suggesting that there was no re-bleaching during the colluviation and pedogenesis associated with the PB-SSU. The significant time interval (~4.8 kyr) separating formation of the PB-SSU and earliest accumulation of LC (Figs 5C and 11) suggests the boundary represents a disconformity. The ROSL-04 age indicates earliest accumulation of LC behind PB2 occurred 7.7 ± 0.8 ka (Fig. 5C). An age of 2.8 ± 0.3 ka for ROSL-03 (located above) suggests that sediment accumulation upslope of PB2 did not occur as a single event (i.e. landslide).

PB3

ROSL-09 (5.8 ± 0.5 ka) (Fig. 6C) is the youngest luminescence age within the PB-SSU among the four studied prehistoric boulders. The OSL age for ROSL-08 suggests earliest accumulation of LC behind (i.e. upslope) PB3 occurred 2.9 ± 0.3 ka (Fig. 6C). Radiocarbon dates come from three charcoal samples from the lowest horizon of LC_R (Fig. 6C, Table 2; Figs S3–5). The 2σ calibrated ages (calendar years AD) range from AD 1661 to AD 1950, with the highest sub-interval probability from AD 1724 to AD 1809 for Rap-CH01 (70.4% of area), AD 1722 to AD 1810 for Rap-CH03 (63.8%) and AD 1732 to AD 1802 for Rap-CH05 (79%). A fire event (or sequence of events) occurring sometime between ~AD 1722 and AD 1810 pre-dates European settlement and is consistent with localized burning during the late Maori Period (~AD 1600–1840) as proposed by McWethy *et al.* (2010). Assuming sediment deposition occurred shortly after burning (and death) of slope vegetation, earliest LC_R accumulation occurred between ~200 and 300 years ago. Charcoal stratigraphically above the dated samples was associated with fragments of baked volcanic rock or possibly brick/pottery mixed with charcoal, potentially indicative of a later phase of European burning (Fig. 6C).

PB4

Quartz OSL ages in PB4 PB-SSU are 13.4 ± 1.2 ka (ROSL-12) and 10.3 ± 1.1 ka (ROSL-11) (Fig. 7C). We interpret these ages as representing primary loess accumulation, but cannot preclude the possibility that the ROSL-11 age reflects bleaching during post-accumulation reworking within PB-SSU. Luminescence ages obtained above and below the PB-SSU/LC boundary suggest a depositional hiatus of ~6 kyr (Fig. 11). Luminescence dating indicates earliest LC accumulation occurred 4.2 ± 0.4 ka (Fig. 7C). The radiocarbon age from charcoal sample Rap-CH06 suggests LC_R sedimentation occurred sometime between AD 1677 and AD 1950, with the highest 1σ confidence interval occurring between AD 1799 and AD 1950 (Fig. S6).

Table 2. Summary results from radiocarbon dating of charcoal within PB3 and PB4 loess-colluvium wedge sediments at the Rapaki study site.

Sample ID	Boulder location	Exposure unit	NZA lab. no.	$\delta^{13}C$ (‰)	Radiocarbon age (^{14}C a BP)	Calibrated age 2σ (cal a AD)	Probability for each 2σ range (%)	Material
Rap-CH01	PB3	LC_R	56801	28.6 ± 0.2	203 ± 18	AD 1664–1698, **1724–1809**, 1870–1876	22.8, **70.4**, 1.0	Charcoal
Rap-CH03	PB3	LC_R	56802	29.1 ± 0.2	197 ± 17	AD 1666–1700, **1722–1810**, 1838–1845, 1867–1878, 1933–1938, 1946–1950	25.8, **63.8**, 1.3, 2.4, 0.6, 1.1	Charcoal
Rap-CH05	PB3	LC_R	56803	27.9 ± 0.2	222 ± 17	AD 1661–1680, **1732–1802**	15.8, **79.0**	Charcoal
Rap-CH06	PB4	LC_R	60079	26.9 ± 0.2	162 ± 22	AD 1667–1736, **1799–1950**	29.4, **65.7**	Charcoal

NZA, Rafter Radiocarbon Laboratory.

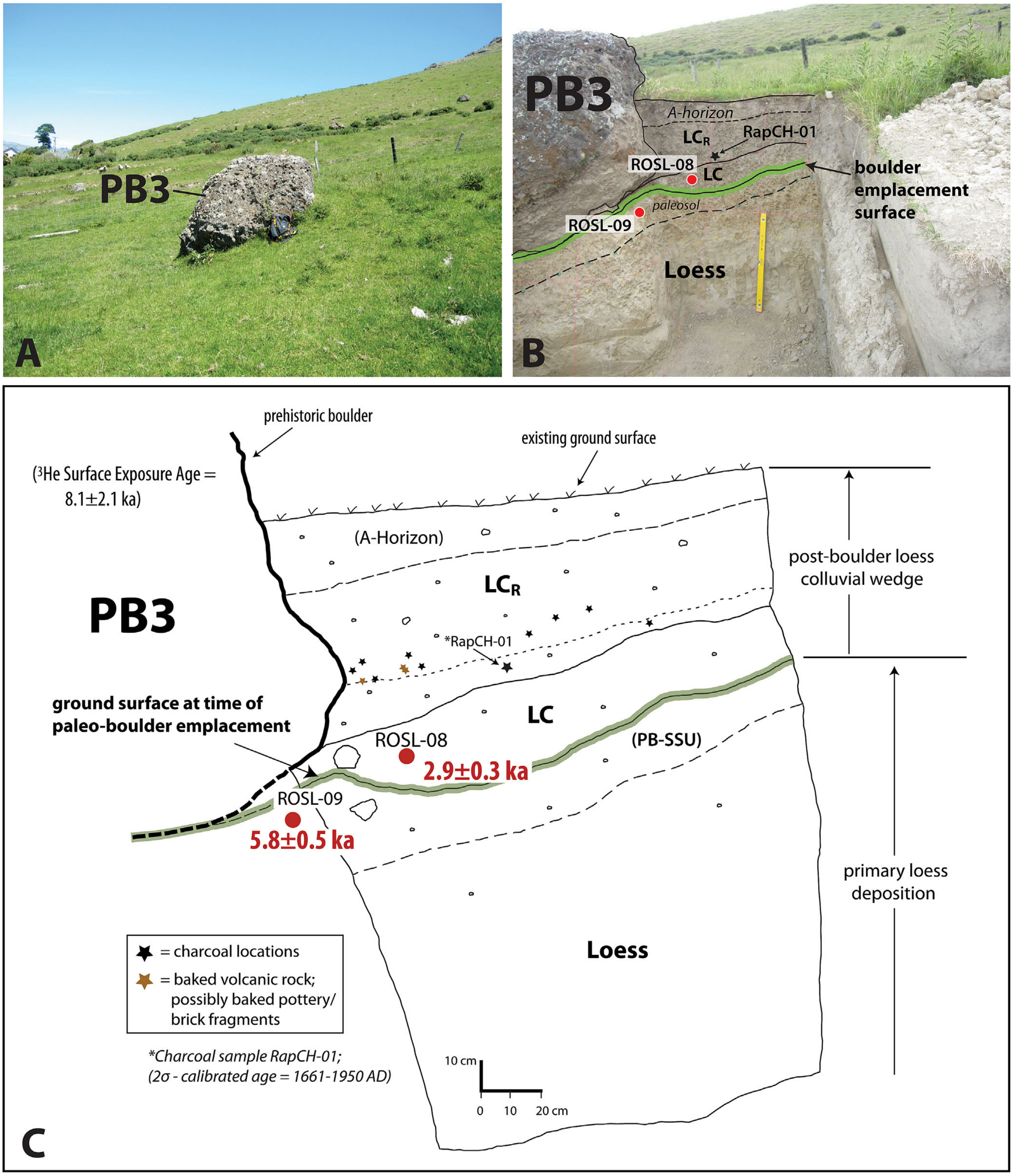

Figure 6. Prehistoric Boulder #3. (A) Photo of PB3 and surrounding hillslope sediment before exploratory trenching. (B) Photo of PB3 exploratory trench with pre-boulder and post-boulder emplacement hillslope sediments exposed. (C) Detailed stratigraphic log of PB3 and surrounding loess and loess-colluvium sediments. OSL (red) and radiocarbon sample location and ages are shown. Mackey and Quigley (2014) ^{3}He surface exposure age for PB3 is also displayed.

PB5

The quartz OSL age at the top of the PB-SSU (ROSL-14) establishes a maximum age of loess accumulation of 10.2 ± 0.8 ka (Figs 8C and 9B). Similar to ROSL-11, we cannot eliminate the possibility that the ROSL-14 age is influenced by bleaching during colluviation and pedogenesis. Initiation of LC deposition upslope of PB5 began 1.7 ± 0.2 ka. Ages from above and below the PB-SSU/LC contact suggest a depositional hiatus of ~8.5 kyr at the PB5 location, the longest of the studied boulders (Fig. 11).

Sediment accumulation rates

Table 4 presents estimates of accumulation rates for PB2–PB5 colluvial wedge sediments. Optical and radiocarbon sample names and ages are shown, as well as the measured stratigraphic thickness between the bracketing ages. Temporal

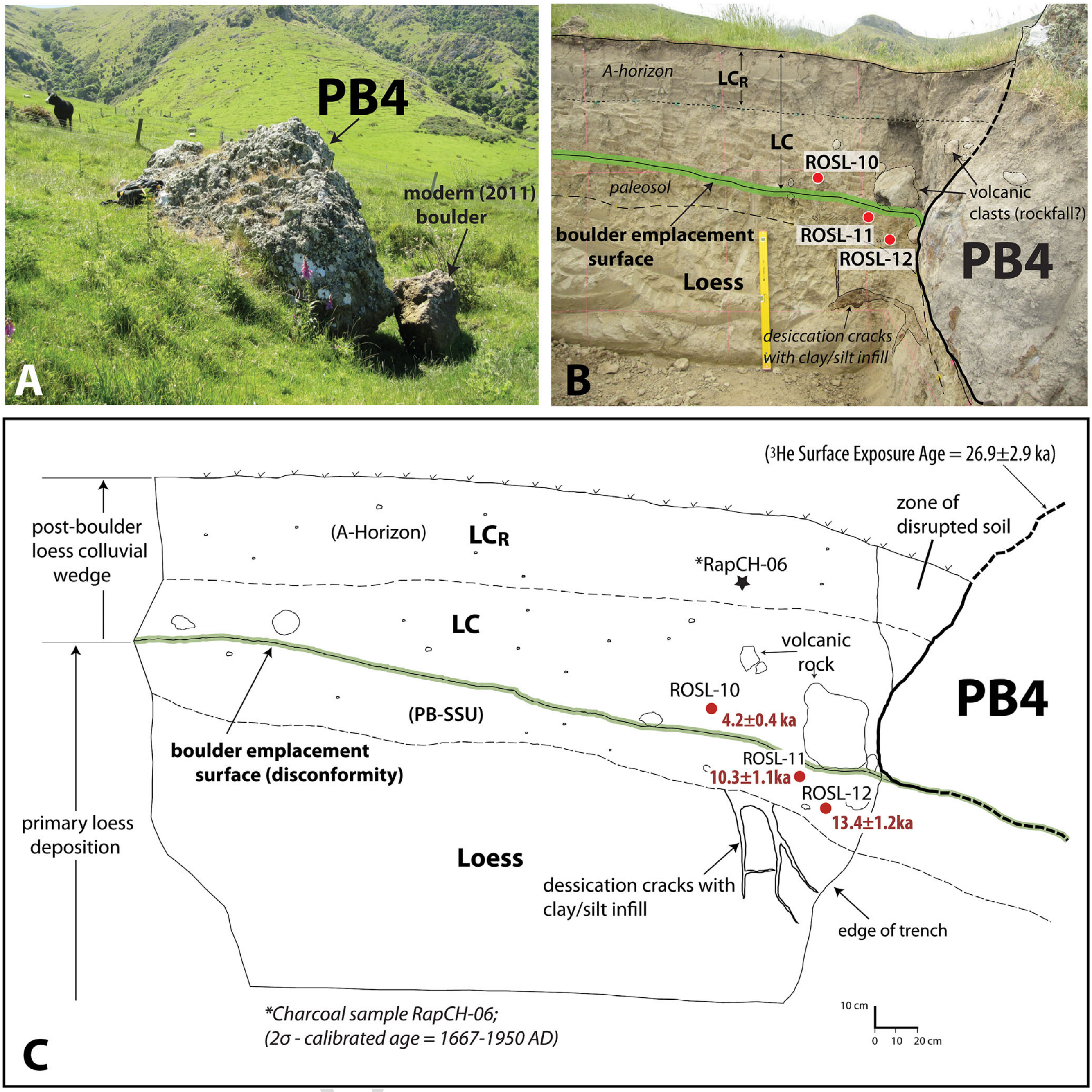

Figure 7. Prehistoric Boulder #4. (A) Photo of PB4 and surrounding hillslope sediment before exploratory trenching. (B) Photo of PB4 and exploratory trench with pre-boulder and post-boulder emplacement hillslope sediments exposed. Meter-stick shown for scale. (C) Stratigraphic log of PB4 and surrounding loess and loess-colluvium sediments. Note the truncation of infilled desiccation cracks at base of Preboulder Soil Stratigraphic Unit (PB-SSU). Quartz OSL and radiocarbon sample locations and ages are shown. Mackey and Quigley (2014) ^{3}He surface exposure age for PB4 is also displayed.

distributions may reflect differences in rates and processes of deposition between near-instantaneous debris and mud flow deposits and more gradual overland flow erosion and deposition. In consideration of this, the deposition rates represent only a first-order linear approximation, but serve to highlight changes in sediment accumulation through time. Our results suggest an overall increase in sediment accumulation rates within loess colluvium moving stratigraphically upward, with a dramatic increase in depositional rate during deposition of LC$_R$.

OSL constraints on timing of boulder emplacement

Quartz OSL ages suggest PB2 was emplaced after 12.5 ± 1.1 ka and before 7.7 ± 0.8 ka (Fig. 11). The top surface of PB2 yielded a surface exposure age of 13.0 ± 2.3 ka (Figs 5C and 10) (Mackey and Quigley, 2014). Assuming the calculated experimental uncertainty for both methods, the CN age and optical overlap can be used to further constrain the emplacement timing of PB2. Combining CN and quartz OSL ages suggests emplacement of PB2 after ~13.6 ka and before ~10.7 ka (Fig. 11). Quartz OSL ages constrain the timing of PB3 to after 5.8 ± 0.5 ka and before 2.9 ± 0.3 ka (Fig. 11). The top surface of PB3 has a CN surface exposure age of 8.1 ± 2.1 ka (Figs 6C and 11). Again, the CN age and luminescence ages show statistical overlap. Combining CN and quartz OSL ages suggests emplacement of PB3 after ~6.3 ka and before ~6.0 ka (Fig. 11). Quartz OSL ages suggest PB4 was emplaced after 10.3 ± 1.1 ka and before 4.2 ± 0.4 ka (Fig. 11). The top surface of PB4 has a CN

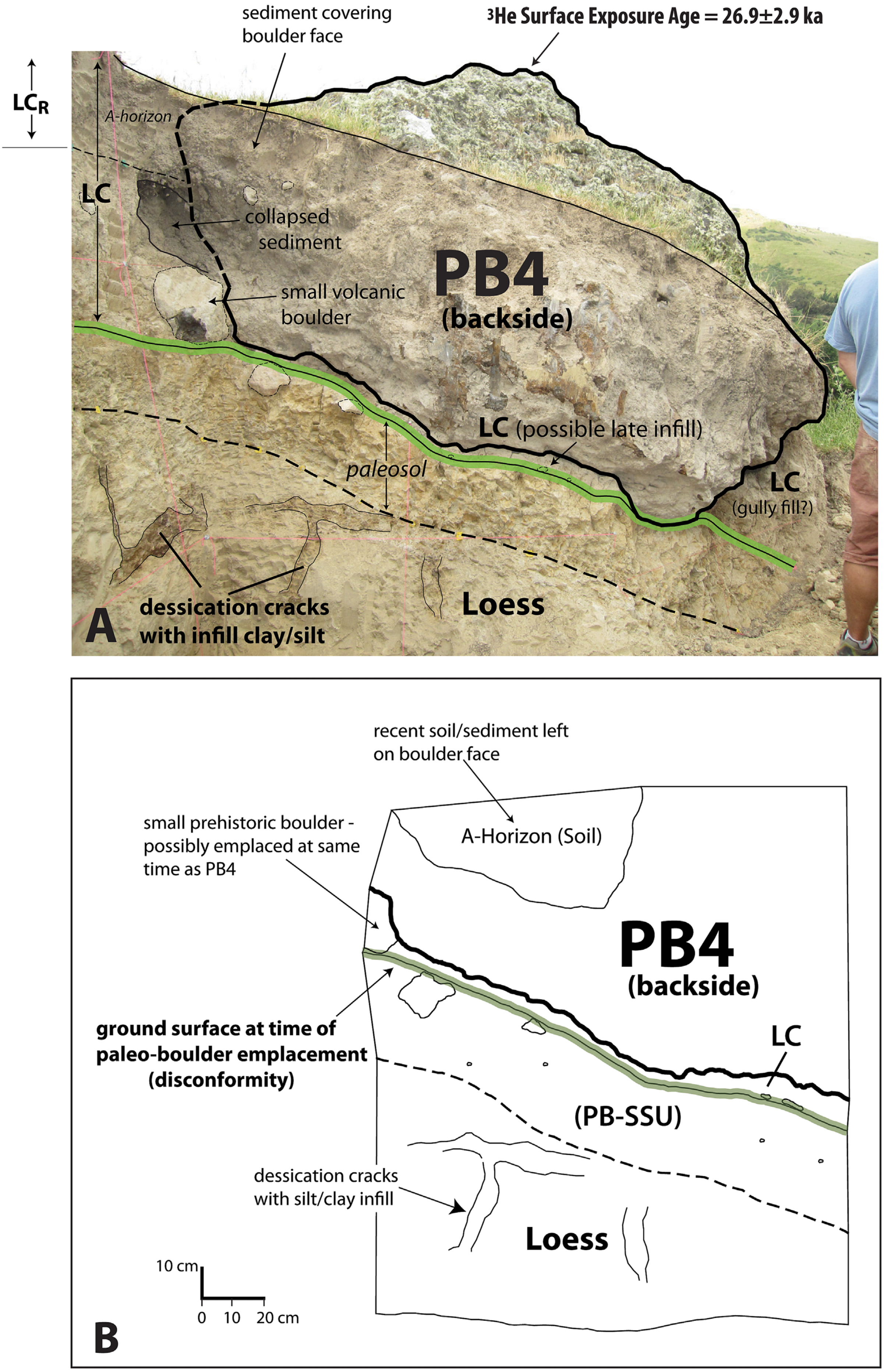

Figure 8. Prehistoric Boulder #4 (PB4). (A) Photo of PB4 backside (upslope) and exploratory trench with pre-boulder and post-boulder emplacement hillslope sediments exposed. Mackey and Quigley (2014) ^{3}He surface exposure age for PB4 is also displayed. (B) Partial stratigraphic log of PB4 (upslope side) and surrounding loess and loess-colluvium sediments.

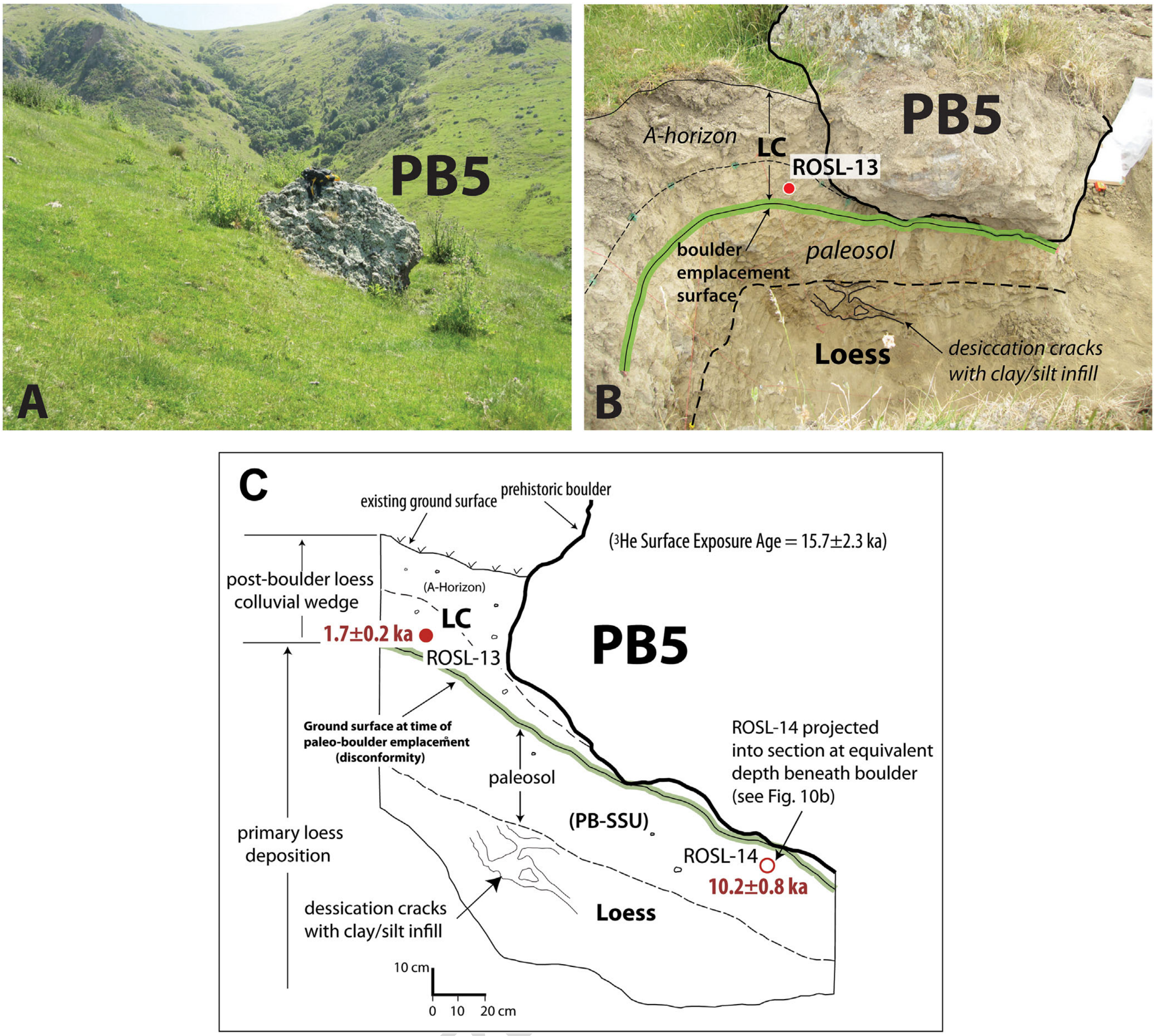

Figure 9. Prehistoric Boulder #5 (PB5). (A) Photo of PB5 and surrounding hillslope sediment before exploratory trenching. (B) Photo PB5 exploratory trench with pre-boulder and post-boulder emplacement hillslope sediments exposed. Note apparent truncation of infilled desiccation cracks at base of PB-SSU zone. (C) Stratigraphic log of PB5 with surrounding loess and loess-colluvium sediments. Quartz OSL sample locations and ages are shown. Mackey and Quigley (2014) ^{3}He surface exposure age for PB5 is displayed at top.

surface exposure age of 26.9 ± 2.9 ka (Figs 7C and 11). The OSL ages are inconsistent with the surface exposure age and suggest strongly that PB4 CN surface exposure age reflects pre-detachment inheritance (Mackey and Quigley, 2014) (Fig. 11). In middle and footslope positions it is likely that any boulder emplaced before ~27 ka would be partially or completely buried beneath loessic sediments. The quartz OSL ages constrain the timing of PB5 to after 10.2 ± 0.8 ka and before 1.7 ± 0.2 ka (Fig. 11). The top surface of PB5 has a CN surface exposure age of 15.7 ± 2.3 ka (Figs 9C and 11). Similar to PB4, the optical ages are inconsistent with the surface exposure age and indicate that the PB5 CN surface exposure age reflects pre-detachment inheritance (Fig. 11).

We used the Bayesian modeling facility of OxCal (v 4.2) (Bronk Ramsey, 2009) to combine OSL and CN ages with stratigraphic information and refine our chronologies (Fig. 12 and Table 5). Figure 12 shows the probability distributions for the OSL and CN boulder ages. CN ages for PB4 and PB5 have been excluded from the analysis because their ages represent clear outliers. PB2 and PB3 minimum and maximum boundary 2σ ages do not overlap and define two distinct rockfall events at 7.0–13.5 ka (Red = E1) and 2.7–6.7 ka (Blue = E2), respectively (Fig. 12). PB4 and PB5 boundary distributions are similar and display statistical overlap with both events, but show slightly stronger agreement with E2, suggesting PB3, PB4 and PB5 could have been emplaced at the same time. We are unable to further constrain the emplacement timing of PB4 and PB5 based upon the OSL ages.

Discussion

Influence of prehistoric rockfall boulders on hillslope process and evolution

Our investigation suggests that the emplacement of large prehistoric boulders on the Rapaki hillslope has locally influenced sediment transport and soil development. We are unaware of any published study in New Zealand or elsewhere that examines this process in the level of detail presented within our study.

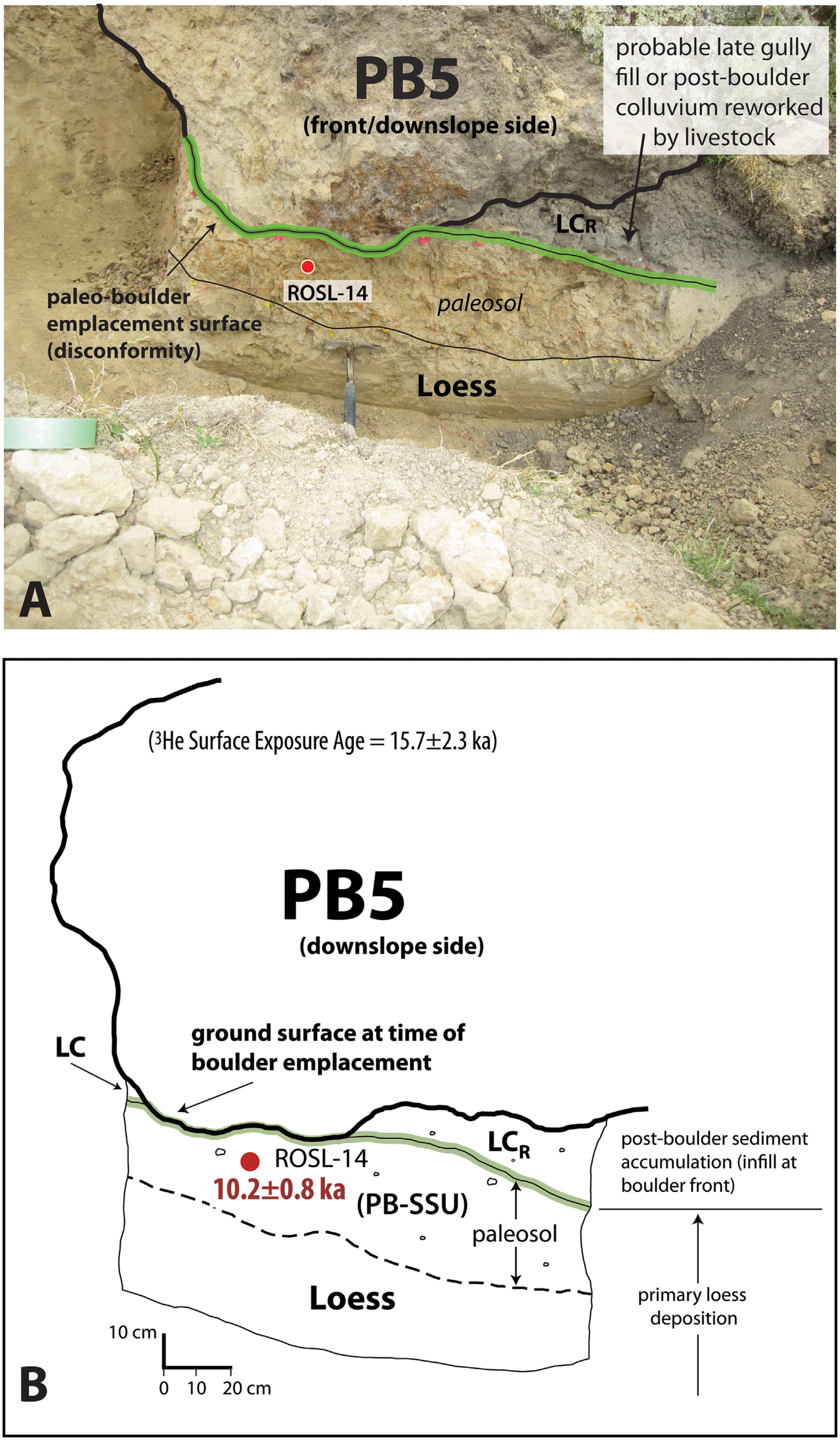

Figure 10. Prehistoric Boulder #5. (A) Photo of PB5 (downslope side of boulder) exploratory trench with pre-boulder and post-boulder emplacement hillslope sediments exposed. (B) Stratigraphic log of PB5 with surrounding loess and loess-colluvium sediments. Quartz OSL sample location and age are shown. Mackey and Quigley (2014) ^{3}He surface exposure age for PB5 is displayed at top.

Table 3. (a) Summary of trench stratigraphy and related field and laboratory measurements for PB2.

Sediment unit	Relative timing	Colour	Texture	Relative moisture	Sediment strength	Bulk density (cm^3)	Thickness (cm)	Structures
Loess	Pre-dates PB2 emplacement	Light yellowish brown (2.5Y 6/4)	Silty loam comprising ~30% sand, 60% silt, 10% clay, very little to no sediment derived from volcanic source rock	Dry	Hard	N/A	97 (min.)	Massive, characteristic gammate structure with gray fissures/veins from desiccation/shrinkage, calcite-filled tubular root structures
PB-SSU	Pre-dates PB2 emplacement	Light olive brown (2.5Y 5/3.5) with dark yellowish brown mottling (10YR 4/6)	Silty loam with minor gravel comprising ~19% sand, 65% silt, 16% clay, slight but notable increase in coarser-grained sediment derived from proximal volcanic source rock, occasional pebble- to cobble-sized clasts of basalt, maximum cobble diameter is ~23 cm	Dry	Hard	1.93–2.04	13–34	Massive, abundant subvertical to vertical cracks with infilling calcite, contains clay coatings (worm castings), intense and pervasive mottling and abundant desiccation cracks, top of PB-SSU marked by disconformity
LC	Post-dates PB2 emplacement	Grayish brown (10YR 5/2) with yellowish brown mottling (10YR 5/2). A-horizon soil is very dark gray (2.5YR 3/1)	Silty loam with gravel to small boulder-sized fragments of volcanic rock (basalt), lower half of LC comprising ~13% gravel, 20% sand, 50% silt, 17% clay, upper half comprising ~2% gravel, 26% sand, 59% silt, 13% clay (% gravel is conservative), significant increase in volcanic derived material, maximum diameter for volcanic rock is 18.87 cm	Damp to semi-moist	Soft to firm	1.59–1.92	110–128	Massive to very poorly layered, A-horizon soil (16–25 cm thick) is intensely altered and bioturbated, abundant small voids (dissolved roots, burrows)
IF-1	Post-dates PB2 emplacement	Light gray (2.5Y 7/2) to light olive brown (2.5Y 5/4) with dark yellowish brown mottling (10YR 4/6)	Silty loam	Damp to dry	Stiff to very stiff	N/A	N/A	Laminations to thin layering (mm to cm scale) parallel to rear surface of PB2, minor rootlets and small mm-scale voids from burrowing
IF-2	Post-dates PB2 emplacement	Very dark gray (2.5Y 3/1)	Silty loam	Damp to semi-moist	Soft to firm	N/A	N/A	No obvious layering, less oxidized than IF-1, small rootlets and mm-scale voids

*PB-SSU is 'Preboulder Soil Stratigraphic Unit' developed in top section of loess.

Table 3. (b) Summary of trench stratigraphy and related field and laboratory measurements for PB3.

Sediment Unit	Relative timing	Colour	Texture	Relative moisture	Sediment strength	Bulk density (cm^3)	Thickness (cm)	Structures
Loess	Pre-dates PB3 emplacement	Light yellowish brown (2.5Y 6/3) to light olive brown (2.5Y 5/4)	Silty loam comprising ~36% sand, 51% silt, 13% clay, very little to no sediment derived from volcanic source rock	Dry	Hard	N/A	133 (min.)	Massive, small vertical to subvertical desiccation cracks observed but not abundant, calcite-filled tubular root structures, some mottling (iron oxidation)
PB-SSU	Pre-dates PB3 emplacement	Grayish brown (2.5Y 5/2) to light olive brown (2.5Y 5/3)	Silty loam with minor gravel comprising ~28% sand, 58% silt, 14% clay, slight but notable increase in coarser-grained sediment derived	Dry	Hard	1.9–2.01	17–34	Massive, tiny mm-scale voids (e.g. burrows, dissolved roots), paleosol development not as advanced compared with PB2/PB4/PB5,

continued

Table 3. (*Continued*)

Table 3. (b) Summary of trench stratigraphy and related field and laboratory measurements for PB3.

Sediment Unit	Relative timing	Colour	Texture	Relative moisture	Sediment strength	Bulk density (cm^3)	Thickness (cm)	Structures
		with yellowish brown mottling (10YR 5/8)	from proximal volcanic source rock, occasional pebble- to cobble-sized clasts of basalt, maximum cobble diameter is ~8.8 cm					occasional old worm burrows with clay coatings and desiccation cracks observed, top of PB-SSU is marked by disconformity
LC	Post-dates PB2 emplacement	Brown to grayish brown (10YR 5/2) with brownish yellow (10YR 6/8) mottling	Silty loam with minor gravel, slight increase in coarse-grained sand and gravel, occasional pebbles/small cobbles of basalt, LC sediment significantly less dense than underlying loess	Damp to semi-moist	Soft to firm	1.27–1.59	24. LC comparatively thin	Massive to very poorly layered, abundant mottling, tiny rootlets pervasive
LC_R	Post-dates PB2 emplacement	Grayish brown (2.5Y 5/2) to very dark gray (2.5Y 4/1). A-horizon soil is very dark gray (2.5Y 3/1)	Silty loam comprising ~24% sand, 64% silt, 12% clay with minor gravel, charcoal abundant, small fragments of charred brick/pottery	Dry to slightly damp	Soft	1.27	70	Moderately to poorly layered, abundant roots and other organic matter (e.g. wood, charcoal), charcoal primarily observed within the lower 30 cm of LC_R, no infill episodes observed adjacent to PB3

Table 3. (c) Summary of trench stratigraphy and related field and laboratory measurements for PB4.

Sediment unit	Relative timing	Color	Texture	Relative moisture	Sediment strength	Bulk density (cm^3)	Thickness (cm)	Structures
Loess	Pre-dates PB4 emplacement	Light yellowish brown (2.5Y 6/3) to light olive brown (2.5Y 5/3)	Sandy loam comprising ~53% sand, 35% silt, 12% clay, we note increased sand % for PB4 loess	Dry	Hard	N/A	155 (min.)	Massive, desiccation cracks infilled with dark brown translocated clay, infilled cracks are part of prismatic structure and taper (i.e. become thinner) with depth, cracks are vertical to subvertical and horizontal to subhorizontal, maximum width for desiccation cracks is ~3.5 cm, calcite-filled root structures, tiny rootlets
PB-SSU	Pre-dates PB4 emplacement	Olive brown (2.5Y 4/3) with dark yellowish brown (10YR 4/6) mottling	Silty loam comprising ~35% sand, 49% silt, 16% clay with minor gravel, increase in coarse-grained sand and gravel sized material derived from the volcanic source rock, several subangular to subrounded, pebble- to small cobble-sized basalt clasts, maximum cobble diameter is ~11 cm.	Dry to damp	Hard	2.17	18–39	Massive, well-developed paleosol with pervasive mottling (iron oxidation), clay coatings with worm castings abundant, top of PB-SSU is marked by a disconformity
LC	Post-dates PB4 emplacement	Grayish brown (10YR 5/2) to dark grayish brown (2.5YR 4/2) with dark yellowish brown (10YR 3/6) mottling	Silty loam comprising ~24% sand, 57% silt, 19% clay with minor gravel, gravel-sized 'stones' (3–6 mm diameter) are commonly encountered within the predominantly silty matrix. Grades upward into silty loam consisting of ~19% sand, 66% silt, 15% clay with minor gravel	Damp to semi-moist	Soft to firm	1.63–1.94	100	Massive to very poorly layered, abundant mottling, small rootlets pervasive, thin white lamination layer (~2–3 mm thick) is observed at depth of ~50 cm. 1–2 mm fragment of charcoal logged at depth of ~33 cm. Upper 35–52 cm of LC may be time equivalent PB3 LC_R sediments
IF-1	Post-dates PB4 emplacement	Dark gray (2.5YR 3/1)	Silty loam, similar in character to PB2 IF-2	Damp to semi-moist	Soft to firm	N/A	N/A	No obvious layering, small rootlets and mm-scale voids

Table 3. (d) Summary of trench stratigraphy and related field and laboratory measurements for PB5.

Sediment unit	Relative timing	Colour	Texture	Relative moisture	Sediment strength	Bulk density (cm^3)	Thickness (cm)	Structures
Loess	Pre-dates PB2 emplacement	Light yellowish brown (2.5YR 6/3) to light olive brown (2.5YR 5/4)	Silty loam comprising ~39% sand, 50% silt, 11% clay	Dry	Hard	N/A	83 (min.)	Massive, desiccation cracks near top infilled with clay/silt, burrowing, calcite-filled root structures
PB-SSU	Pre-dates PB2 emplacement	Light yellowish brown (2.5YR 6/3) with yellowish brown mottling (10YR 4/6)	Silty loam comprising ~26% sand, 62% silt, 12% clay; small increase (relative to in situ loess) in volcanic derived subangular to subrounded, coarse-grained sand and gravel	Dry	Hard	1.83	29–44	Massive, subvertical to vertical desiccation cracks commonly filled with calcite, well-developed paleosol with abundant mottling (iron oxidation), contains clay-coated worm casts, top of PB-SSU marked by disconformity
LC	Post-dates PB2 emplacement	Grayish brown (10YR 5/2), within A-horizon very dark gray (2.5YR 3/1)	Silty loam with minor gravel comprising ~32% sand, 55% silt, 13% clay; relative increase in coarse-grained sand and gravel. A-horizon soil is silty loam comprising ~31% sand, 58% silt, 11% clay	Dry to damp	Soft to firm	1.30	37–47. A-horizon is 17–34 cm	Massive to very poorly layered, A-horizon soil intensely altered and bioturbated, abundant small voids (dissolved roots, burrows)

At the time loess accumulation ceased or dramatically slowed at *ca.* 13 ka (see below), the hillslope at Rapaki shifted from being net aggradational to erosional. Coincident with this transition, soil evolution shifted from upbuilding during loess accumulation (Johnson *et al.*, 1987; Johnson and Watson-stegner, 1987) to topdown (Almond and Tonkin, 1999) during downwasting (Fig. 13A). The (buried) soil in the top of the loess beneath each of the studied prehistoric boulders (PB-SSU) preserves the mobile colluvial biomantle (Johnson, 1990; Heimsath *et al.*, 2001, 2002; Johnson *et al.*, 2005) by which downwasting was achieved (Fig. 12A). Its morphology suggests a soil residence time (Almond *et al.*, 2007a) in the order of many hundreds of years to millennia, and hence relative slope stability. We propose that the small percentage of coarser-grained volcanic sediment observed within PB-SSU was incorporated into the loess through a variety of surface hillslope transport processes (e.g. bioturbation, shallow debris and mud flows, local overland flow transport). Reworking of infilled desiccation cracks within the upper loess section for PB4 and PB5 supports our assertion that the PB-SSU was an active soil layer which underwent vigorous pedoturbation (Figs 7C and 9B,C).

The emplacement of large prehistoric boulders on the Rapaki hillslope facilitated a return to localized aggradational hillslope process, by (i) creating accommodation space (i.e. sediment barrier/trap) for sediment accumulation and (ii) effectively ‘locking-in’ or ‘immobilizing’ sections of the previously mobile soil layer (i.e. PB-SSU) lying directly below and upslope of the boulder (Fig. 12B). Once the boulder is emplaced and the underlying mobile soil layer ‘fixed’, sediment deposition may begin, with the rate of sediment accumulation depending on the boulder’s topographic position, amount of available sediment and the mechanism of deposition (e.g. mass wasting, creep, overland flow) (Fig. 13B). Soil evolution again becomes upbuilding in character, although depositional events are more discrete and stochastic than the earlier loess upbuilding phase. The soil in colluvial wedge sediments upslope of the boulders is characterized by a series of stacked A-horizons with small rootlets and worm burrows evident throughout. The absence of B-horizons indicates a relatively rapid rate of accumulation so that upbuilding was effectively retardant (Johnson and Watson-stegner, 1987).

We propose that the combined influence of boulders (and associated smaller sized rockfall debris) on hillslope process and resulting surface morphology may be underestimated, particularly in middle to upper slope positions, where spatial density of rockfall is high. Field observations reveal hummocky terrain in middle and upper slope positions that could be attributed to a combination of surficial landsliding and creep. However, we speculate that this geomorphic signature may be at least partially influenced by abundant prehistoric boulders lying beneath and at the surface. Build-up of sediment behind boulders and erosion adjacent to boulders could conceivably create a similar morphological pattern. Further surface and subsurface investigation is required to determine the influence that boulders have on hillslope process and geomorphic pattern.

Summary of landscape evolution at Rapaki

Based on a synthesis of the OSL age distributions from loessic sediments, our favored hypothesis is that loess accumulation occurred in at least some areas of the study site until *ca.* 12–13 ka at the earliest. ROSL-06 is located within the *in situ* loess at a depth of ~30 cm below the paleo-ground surface and yields an age of 12.0 ± 1.4 ka (Fig. 5). ROSL-05 is

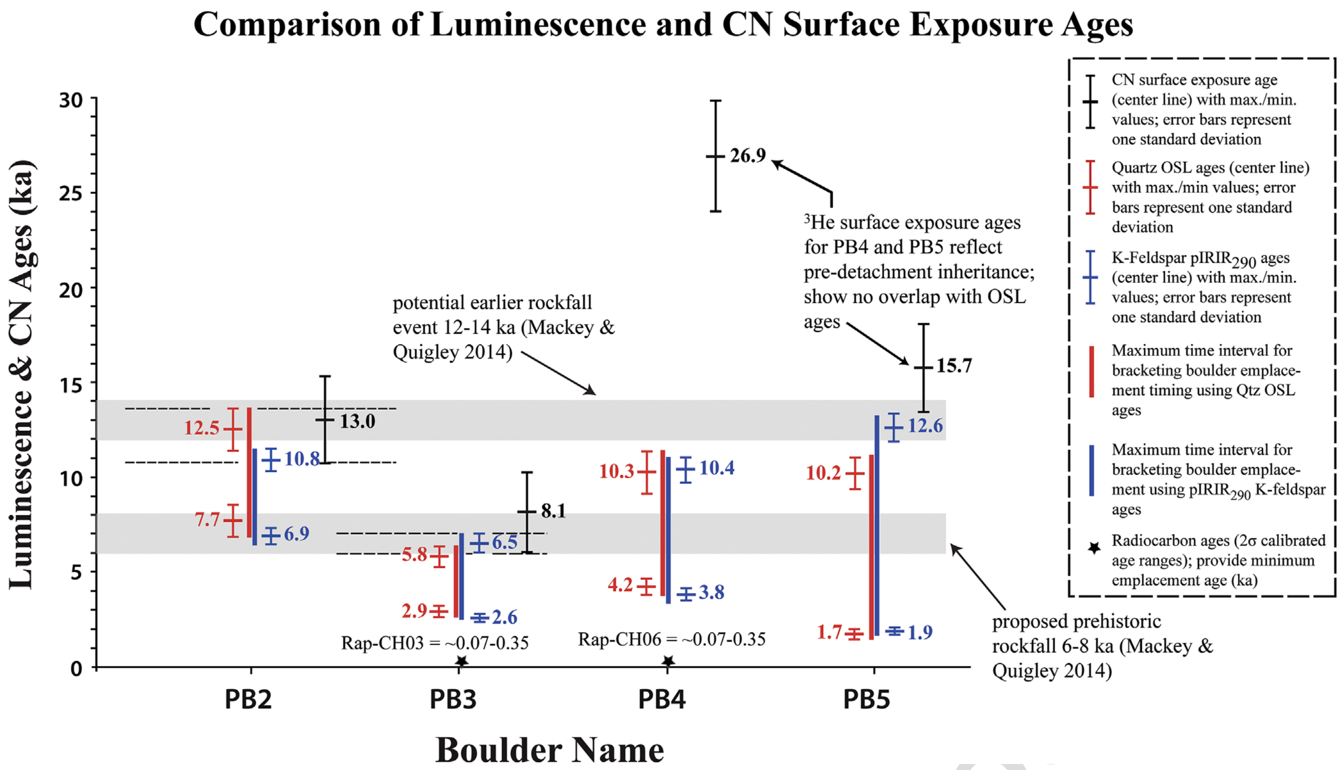

Figure 11. Luminescence ages are compared with CN surface exposure ages from the top surface of the prehistoric boulders (Mackey and Quigley, 2014). Both quartz OSL and K-feldspar pIRIR$_{290}$ maximum and minimum emplacement ages are shown for each of the prehistoric boulders. Radiocarbon ages (calibrated 2σ range) for PB3 and PB4 are also shown for comparison.

located near the top of the loess section (above ROSL-06) within PB-SSU and yields a statistically overlapping age of 12.5 ± 1.1 ka (Fig. 5). ROSL-12 within PB4 PB-SSU yields a statistically overlapping age of 13.4 ± 1.2 ka. How much later loess accumulation continued is indeterminate from our work because the resulting deposits may have been eroded. Although Almond *et al.* (2007b) report an IRSL age of 1860 years in the upper 40 cm of loess at Ahuriri Quarry, this age is likely to be much younger than the depositional age because of post-depositional bleaching during bioturbation and hillslope soil transport. The sources for the loess of Banks Peninsula are the outwash plains of the major rivers to the west that flow across the Canterbury Plains. The closest currently is the Rakaia River, which began its incision about 13 ka. The timing of incision comes from a thermoluminescence age from the base of loess above outwash gravels (Berger *et al.*, 1996). This loess thins rapidly away from the Rakaia River to the south (Ives, 1973) forming a local loess wedge. The incision of the Rakaia River, if synchronous with the other glacially fed rivers of the plains, is therefore likely to mark the beginning of a period of much reduced loess flux.

It is possible the younger luminescence ages within PB-SSU (e.g. ~10 ka ages for ROSL-11, ROSL-14) reflect loess depositional ages or near surface reworking (e.g. bioturbation,

Table 4. Summary of sediment accumulation rates in post-boulder emplacement colluvial sediments, including sample name and ages used for rate determination, and measured stratigraphic thickness between samples. Quartz OSL ages used to determine approximate sediment accumulation rates. 2σ calibrated highest probability ranges (Table 2) used to estimate age and determine sediment accumulation rates for RAP-CH01 and RAP-CH06.

Boulder/ trench	Unit	Sediment accumulation rate (mm a^{-1})	Luminescence and radiocarbon samples used for rate determination	Time between bracketing samples (years)	Measured stratigraphic thickness between samples (mm)
PB2	LC	*Upper LC* 0.23 ± 0.02	ROSL-03; existing ground surface (t = 0)	2800 ± 300	640
		Lower LC 0.07 ± 0.02	ROSL-04; ROSL-03	4900 ± 1100	360
PB3	LC$_R$	2.21 ± 0.39	RAP-CH01; existing ground surface (t = 0)	~249 ± 44*	532
	LC	0.05 ± 0.01	ROSL-08; RAP-CH01	2651 ± 344	128
PB4	LC$_R$ (?)	3.26 ± 1.76	RAP-CH06; existing ground surface (t = 0)	~141 ± 76	326
	LC	0.12 ± 0.015	ROSL-10; RAP-CH06	4059 ± 476	497
	LC (assuming no LC$_R$ deposition)	0.22 ± 0.02	ROSL-10; existing ground surface (t = 0)	4200 ± 400	926
PB5	LC	0.18 ± 0.02	ROSL-13 & existing ground surface (t = 0)	1700 ± 200	304

Quartz luminescence ages used to determine sediment accumulation rate; *ages from radiocarbon dating of charcoal samples.

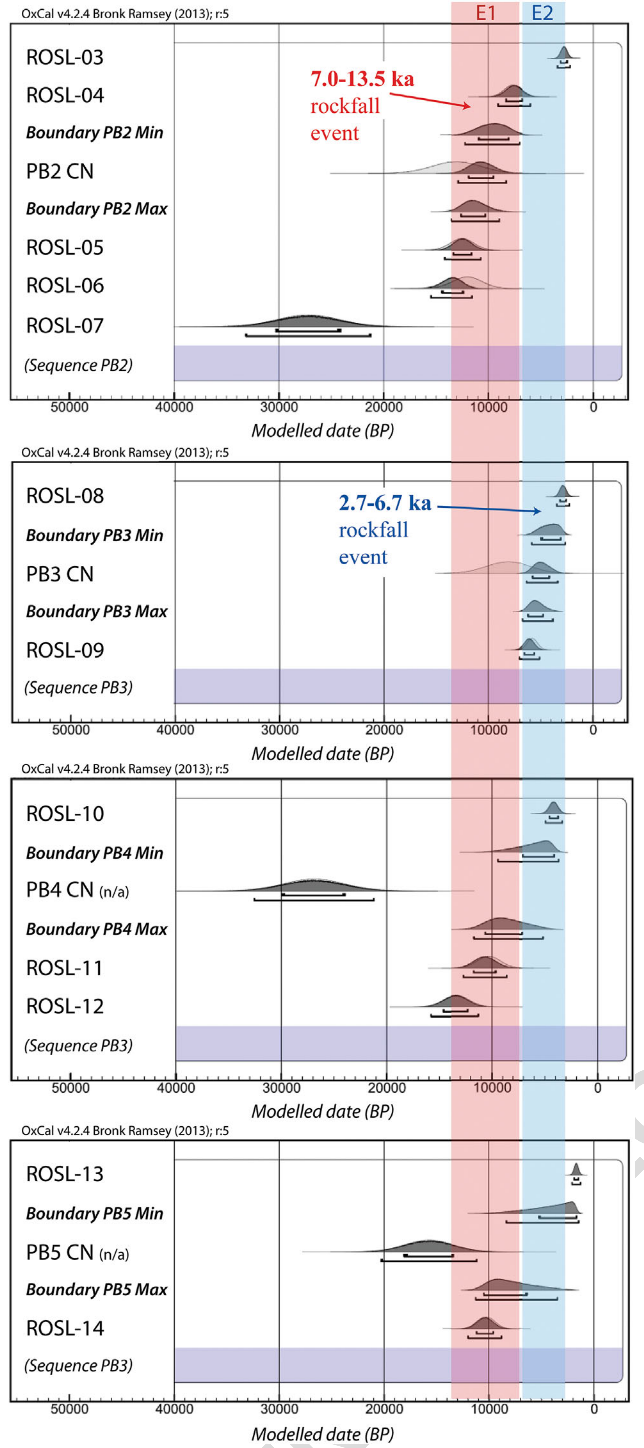

Figure 12. Bayesian modeled probability distributions (using OxCal) for luminescence and CN ages. PB2 and PB3 2σ minimum and maximum boundary ages do not overlap and define two distinct rockfall events at 7.0–13.5 ka (red = E1) and 2.7–6.7 ka (Blue = E2), respectively. PB4 and PB5 boundary distributions are similar and display statistical overlap with both events, but show slightly stronger agreement with E2, suggesting PB3, PB4 and PB5 could have been emplaced at the same time.

tree throw, pedogenic mixing) of the ~12–13-ka and older loess. Although the consistency between quartz and feldspar suggests (Table 1, Fig. 11 and Sohbati *et al.*, 2016) these may reflect *in situ* accumulation ages, we cannot dismiss the possibility that they result from resetting of the luminescence signal during near surface mixing. Further investigations involving single grain luminescence methods would be required to resolve whether these reflect deposition ages or not. With regard to ROSL-09 (5.8 ± 0.5 ka), there are three-dimensional stratigraphic complexities (i.e. a possible undulating PB-SSU/LC contact) that mean we cannot exclude the possibility that sampling punctured through the PB-SSU layer into LC. Hence, we cannot dismiss the possibility that OSL sampling represents a mixture of PB-SSU and LC sediments, and as a result we cannot be confident that this age is a meaningful loess depositional age.

Latest loess accumulation and earliest deposition of loess colluvium (LC) is separated by a depositional hiatus (disconformity) ranging from ~3 to 9 kyr, suggesting multi millennial-scale periods of non-deposition and/or erosion on the Rapaki landscape. Earliest onset of loess colluvium deposition behind the studied prehistoric boulders ranges from ~7.7 to ~1.7 ka (mid-Holocene), with accumulation and preservation contingent upon boulder presence.

We observe a significant pulse of sedimentation (behind PB3 and PB4) that occurs synchronously with human arrival and residence in the study area. We attribute this sediment increase to anthropogenic deforestation sometime between AD 1661 and AD 1950 (2σ calibrated age ranges), which destabilized the land surface and facilitated more hillslope erosion and re-deposition of sediment. Although we cannot rule out natural fire as a cause of deforestation, the onset of increased colluvial sedimentation during the period of local human colonization, widespread evidence for anthropogenic deforestation elsewhere in the region and absence of modern forest cover suggest human sustainment of an unforested landscape since the 17th to earliest 20th century (Borella *et al.*, 2016). Similar responses to deforestation have been observed at other sites in New Zealand (e.g. Kasai *et al.*, 2005; Kettner *et al.*, 2007) and globally (e.g. Syvitski *et al.*, 2005).

Temporal constraint of boulder emplacement using OSL method

Optical dating of loessic hillslope sediments can be used to successfully constrain the timing of prehistoric boulder emplacement (Sohbati *et al.*, 2016), which under certain circumstances may be used as a proxy for the timing of prehistoric earthquakes (Mackey and Quigley, 2014). We are aware of only a handful of published studies globally (e.g. Matmon *et al.*, 2005; Chapot *et al.*, 2012; Rinat *et al.*, 2014) that use OSL dating of hillslope sediments to date prehistoric rockfall events. These studies focus on OSL dating of sediments either below or behind the rockfall boulders (in support of other dating techniques, *e.g.* radiocarbon, CN exposure dating), but do not combine OSL dating of both pre- and post-boulder fall sediments (for a single boulder) to constrain emplacement timing. At Rapaki, the influx of loessic sediments into the hillslope system (primarily during the Pleistocene) provides a significant volume of sediment for remobilization and eventual deposition behind rockfall boulders. At Rapaki, temporal constraints using the OSL method are controlled by two primary factors: (i) the timing of boulder emplacement and (ii) the episodic and spatially irregular nature of hillslope sedimentation.

Luminescence ages within PB-SSU provide estimates of maximum boulder emplacement age. Determining the amount of time elapsed between PB-SSU deposition and boulder emplacement on top of PB-SSU (i.e. paleo-ground surface) is difficult. Sediments accumulated upslope of the boulder provide a minimum age for boulder emplacement because their deposition (and preservation) can occur only once the boulder is present. However, sediment accumulation may significantly post-date boulder emplacement. If

Table 5. Summary of unmodeled and modeled ages for luminescence and CN surface exposure ages using Bayesian modeling facility of OxCal (v 4.2) (Ramsey, 2009). 2σ age ranges are highlighted (bold) for boundary minimum and maximum ages. Modeled CN ages for PB4 and PB5 have been excluded from the analysis (see Fig. 12) because they are inconsistent with the stratigraphy/OSL chronologies.

	Unmodeled (BP)						Modeled (BP)					
Name	From	To	%	From	To	%	From	To	%	From	To	%
Sequence PB2												
ROSL-03	3101	2500	68.2	3400	2200	95.4	3103	2503	68.2	3402	2205	95.4
ROSL-04	8500	6900	68.2	9296	6104	95.4	8324	6734	68.1	9087	5974	95.4
Boundary PB2_min							10 943	8072	68.2	***12 206***	***7023***	***95.4***
PB2CN	15 300	10 701	68.2	17 590	8410	95.4	11 858	9514	68.2	12 864	8302	95.4
Boundary PB2_max							12 583	10 288	68.2	***13 511***	***8964***	***95.4***
ROSL-05	13 600	11 400	68.2	14 695	10 305	95.4	13 332	11 595	68.2	14 170	10 719	95.4
ROSL-06	13 400	10 600	68.2	14 795	9205	95.4	14 427	12 363	68.1	15 476	11 554	95.4
ROSL-07	30 198	24 203	68.2	33 186	21 215	95.4	30 273	24 115	68.2	33 156	21 218	95.4
Sequence PB3												
ROSL-08	3201	2600	68.2	3500	2300	95.4	3166	2557	68.2	3455	2265	95.4
Boundary PB3_min							4989	3085	68.1	***5850***	***2663***	***95.4***
PB3CN	10 200	6000	68.2	12 290	3910	95.4	5768	4165	68.3	6327	3362	95.4
Boundary PB3_max							6210	4749	68.2	***6726***	***3808***	***95.4***
ROSL-09	6300	5300	68.2	6799	4802	95.4	6574	5598	68.3	7040	5110	95.4
Sequence PB4												
ROSL-10	4600	3800	68.2	5000	3401	95.4	4542	3739	68.2	4930	3341	95.4
Boundary PB4_min							7063	4117	68.2	***9424***	***3695***	***95.4***
PB4CN	29 798	24 002	68.2	32 687	21 114	95.4	29 896	23 969	68.2	32 559	21 224	95.4
Boundary PB4_max							10 642	7109	68.2	***11 698***	***5165***	***95.4***
ROSL-11	11 400	9200	68.2	12 495	8105	95.4	11 723	9643	68.1	12 684	8616	95.4
ROSL-12	14 600	12 200	68.2	15 795	11 005	95.4	14 616	12 279	68.2	15 783	11 279	95.4
Sequence PB5												
ROSL-13	1901	1500	68.2	2100	1300	95.4	1889	1489	68.2	2089	1285	95.4
Boundary PB5_min							5196	1666	68.2	***8333***	***1468***	***95.4***
PB5CN	18 000	13 401	68.2	20 290	11 110	95.4	18 088	13 372	68.3	20 267	11 153	95.4
Boundary PB5_max							10 475	6323	68.2	***11 251***	***3475***	***95.4***
ROSL-14	11 000	9400	68.2	11 796	8604	95.4	11 174	9587	68.2	11 970	8804	95.4

Performed using Bayesian modeling facility of OxCal (v 4.2).

sediment accumulation occurs during or shortly after boulder emplacement, then luminescence ages within the lowest LC sediments provide the best estimate of the timing of boulder emplacement. At Rapaki, maximum and minimum bounding OSL ages suggest there are long periods of non-deposition and erosion on the hillslope, ranging from ~3 to 9 kyr in the boulder locations.

The temporal resolution for boulder emplacement timing could possibly be improved by sampling sediments closer to the PB-SSU contact (i.e. prehistoric boulder emplacement surface), although sampling near a former surface may be problematic because of bioturbation. Our results indicate areas that are topographically high (i.e. divergent zones) and receive low sediment input are less desirable (e.g. PB5 location) for using luminescence dating to constrain the timing of boulder emplacement. Boulders located in drainage valleys/gullies (i.e. convergent zones) should be avoided because of potential boulder mobility issues and depositional complexities (i.e. frequent deposition and removal of sediment behind boulders).

We note that OSL dating of infill sediments behind prehistoric boulders could provide an independent method for constraining major prehistoric shaking events, as it is difficult to envisage a cause other than earthquakes (Khajavi *et al.*, 2012) for episodic displacement (albeit small) of such large boulders. Assuming each of the infills is related to a seismically induced displacement, PB2 (Fig. 5B,C) may potentially record two separate shaking events (i.e. 2011 and a previous prehistoric shaking episode).

Summary and comparison of OSL and CN ages

When the entire suite of OSL ages across the study site are considered and compared to the corresponding suite of CN ^{3}He boulder exposure ages, several general interpretations can be drawn. PB2, PB4 and PB5 overlie loessic sediment that yields OSL ages of ~10.2–12.5 ka, suggesting that boulder emplacement occurred during or after this time. The development and disturbance of a paleosol at the top of the loessic sediments (and beneath the boulders) favors the interpretation that boulder deposition occurred *after* loessic sediment aggradation had ceased on the hillslope; we cautiously infer that 100 to 1000s of years would have been required to develop the paleosol in the PB-SSU unit before the boulders were emplaced. Given our lack of confidence in the interpretation of the ROSL-09 sample age (see above) we are reluctant to constrain the maximum emplacement age of PB3 using the ~5.8-ka OSL age. We are similarly cautious about using the OSL age from beneath PB1 alone to constrain the timing of boulder emplacement beyond the conclusion that PB1 was emplaced after 29.3 ka. OSL ages of sediment accumulated

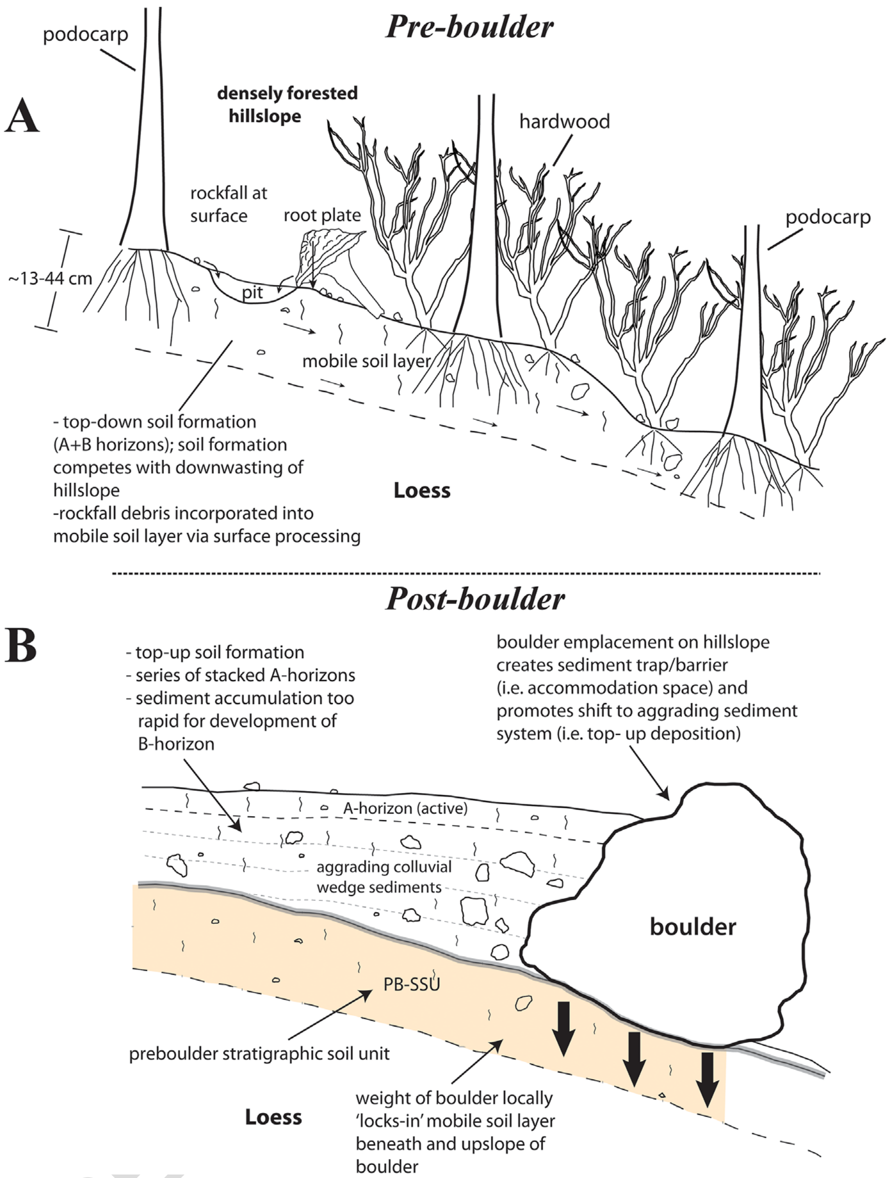

Figure 13. (A) Conceptual diagram for mobile soil layer before emplacement of large prehistoric boulder on Rapaki hillslope. Before boulder deposition, the local sediment system is degradational (i.e. dominated by creep and erosion). Top-down soil formation competes with hillslope downwasting. Soil flux and incorporation of coarse-grained volcanic rock into the physically disturbed soil layer presumably results from surface/subsurface processing including tree-throw, root growth, shallow mass wasting and local overland flow process. (B) Conceptual diagram of post-boulder emplacement sedimentation and soil formation. Boulder emplacement on the hillslope creates two important conditions for accumulation (and preservation) of colluvial wedge sediments: (i) sediment trap/barrier (i.e. accommodation space) and (ii) locally 'locks-in' underlying mobile soil layer beneath and upslope of boulder. Locally, deposition of large boulder changes the sediment system to aggradational. Soil development in PB-SSU stops with accumulation of the sediment behind the boulder. Soil formation behind the boulder is 'top-up' and consists of a series of stacked A-horizons. Sediment accumulation is rapid enough to inhibit B-horizon development.

upslope of the boulders range from ~7.7 to 1.7 ka; when considered collectively, these data imply that boulders were emplaced before this time.

The corresponding CN ^{3}He ages from all boulders are significantly older than all the OSL ages for underlying sediment with the exception of PB2, where CN and OSL ages are within error, and PB1. This relationship of older CN ^{3}He-derived emplacement ages for boulders sitting above younger OSL ages is inconsistent with stratigraphic superposition and requires either that the OSL ages are younger than the true depositional age of the loessic sediment (e.g. Almond *et al.*, 2007b; Grapes *et al.*, 2010a,b), that the CN ages are older than the true timing of boulder emplacement (e.g. Mackey and Quigley, 2014), or both. Our confidence that most of the OSL ages are robust representations of the depositional ages of the sampled sediment is increased by the inter-site age consistency for stratigraphically equivalent sediments, the intra-site adherence of OSL ages to stratigraphic position, and the consistency between quartz OSL and K-feldspar $pIRIR_{290}$ ages (Sohbati *et al.*, 2016). Conversely, in consideration of the entire suite ($n = 19$ boulders) of CN ages from the study site, Mackey and Quigley (2014) concluded that a major rockfall event occurred between *ca.* 6 and 8 ka, with a possible precursor event at *ca.* 13–14 ka, and that older CN ages were interpreted to reflect inherited CN concentrations that accumulated in boulder surfaces before boulder emplacement.

In consideration of these data, we favor the interpretation that PB4 (CN age ~26.9 ka) and PB5 (~15.7 ka) contain significant inherited CN ^{3}He, and that the best temporal constraints on boulder emplacement age are provided by Bayesian modeling of OSL ages from the bounding sediments (Fig. 12). We favor an emplacement age closer to the central *PB4* Min (~5–7 ka) and *PB5* Min (~2–6 ka) estimates (Fig. 12) for the reasons described above, but we cannot absolutely resolve these emplacement ages to this temporal resolution, and boulder emplacement any time after ~10 ka and before 2–4 ka is permissible.

CN ^{3}He ages from PB1 (~11.8 ka) and PB2 (~13 ka) are consistent with OSL ages of the bounding strata. Although ^{3}He inheritance cannot be excluded as influencing age distributions, particularly for PB2 (where the central ^{3}He age is slightly older than the central ages of the underlying loess), we have no evidence to explicitly discredit the CN ages as a proxy for the timing of boulder emplacement. These ages were recorded elsewhere on the study slope and provide tentative evidence for boulder emplacement at ~12–14 ka (Mackey and Quigley, 2014).

Since we are uncertain about the meaningfulness of the ROSL-09 age, we are unable to evaluate the ~8-ka CN ^{3}He age for inheritance. If the ROSL-09 age represents the depositional age of the sediments underlying PB3, then PB3 is likely to have some ^{3}He inheritance, and if the ROSL-09 age underestimates the depositional age of this sediment, then the PB3 age could represent the timing of boulder emplacement age (or not). The occurrence of other ~6–8-ka CN ages at the study site suggests that the PB3 ^{3}He age could provide a reasonable estimate for the timing of boulder emplacement.

The proposed ~6–8-ka and possible 13–14-ka timings of major rockfall events at the study site (Mackey and Quigley, 2014) are not invalidated by the OSL ages. In some cases the OSL dating and stratigraphic mapping supports the proposed timing of these rockfall events. Further coupled analyses of rockfalls and hosting sedimentary sequences throughout this region would be required to further test the validity of this hypothesis. Clearly, this study illustrates both the opportunities and the challenges of constraining the timing of rockfall events and hillslope sedimentation in this setting. Similar challenges will exist in analogous settings elsewhere.

Conclusions

Optical and radiocarbon dating of loessic hillslope sediments enables evaluation of the timing of prehistoric rockfall and provides a reliable temporal framework for the evolution of loess-mantled hillslopes at Rapaki (NZ). Under certain circumstances, our approach may be used to date earthquake-triggered rockfalls and hillslope responses to seismic and anthropogenic influence elsewhere in New Zealand and globally. Rockfall boulders preserve an important record of Holocene hillslope soil transport, and influence local hillslope morphology and soil evolution. In this instance, stratigraphic analysis and OSL dating have provided greater confidence in some previously obtained boulder emplacement ages (derived from CN ^{3}He) and have helped to recognize which CN ^{3}He ages are most likely to overestimate boulder emplacement timing due to CN inheritance. Sediment accumulation rates increased (>~10-fold) following human arrival and associated anthropogenic burning of slope vegetation. Field observations and luminescence ages suggest boulder emplacement and deposition of loess colluvium did not occur concurrently and probably result from different causal mechanisms, implying that seismologic and meteorological phenomena play different roles in shaping the modern landscape. Our study highlights the importance of understanding the roles of earthquakes and humans on surface processes.

Supplementary Material

Fig. S1. (A) Photo of PB1 before exploratory trenching. (B) Photo of PB1 with underlying loessic sediments exposed. An OSL sample (shown) was retrieved within the *in situ* loess and yields a quartz OSL age of 29.3 ± 2.5 ka (Table 1). PB1 is located in an area of active tunnel gully erosion and deposition, and highlights the potential depositional complexities associated with prehistoric boulders on the Rapaki hillslope. Recent tunnel gully fill is found underlying PB1 and older loess deposits.

Fig. S2. Photo of PB6 and adjacent (upslope) exploratory trench. Due to safety concerns, we were unable to expose the boulder base and identify the boulder emplacement surface. OSL sample location (ROSL-15; red circle) shown – sample not dated. PB6 is located within the axis of a drainage valley (Figs 2 and 3) – a zone of active erosion and sediment (and potentially boulder) remobilization. Large volcanic clasts are observed to bottom of trench, indicating deposition by possible debris and mudflow and/or high-velocity water flow. PB6 CN surface exposure age shown at top.

Fig. S3. Radiocarbon calibration report for charcoal sample RapCH-01.

Fig. S4. Radiocarbon calibration report for charcoal sample RapCH-03.

Fig. S5. Radiocarbon calibration report for charcoal sample RapCH-05.

Fig. S6. Radiocarbon calibration report for charcoal sample RapCH-06.

Table S1. Summary of boulder name, volume, elevation, lithology, rounding/shape, lichen cover (moderate to dense = 50–75% cover; dense = >75% cover), surface roughness (low, moderate, high reflect average surface amplitudes of ~<3, ~3–6 and ~>6 cm, respectively), and colluvial wedge thickness.

Table S2. Summary of grain size distribution for PB2–PB5 Rapaki hillslope sediments.

Table S3. Bulk density for loess and loess-colluvial sediments at Rapaki, New Zealand.

Acknowledgements. Financial support for the project came from the EQC (Earthquake Commission) capability fund for South Island geohazards research. J.B. thanks Jarg Pettinga, David Bell, Sam Hampton, Maxwell Borella, and Simon Brocklehurst for field assistance and/or insightful discussions related to Banks Peninsula geology. R.S. thanks the Carlsberg Foundation for financial support (grant no. 2012_01_0838) during the project. The authors declare that they have no competing interests.

Abbreviations. AMS, accelerator mass spectrometry; CN, cosmogenic nuclide; IRSL, infrared-stimulated luminescence; OSL, optically stimulated luminescence; SAR, single-aliquot regenerative-dose.

References

Aitken MJ. 1998. *An Introduction to Optical Dating*. New York: Oxford University Press.

Almond P, Roering J, Hales TC. 2007a. Using soil residence time to delineate spatial and temporal patterns of transient landscape response. *Journal of Geophysical Research* **112**: 1–19.

Almond PC, Roering JJ, Hughes MW *et al.* 2008. Climatic and anthropogenic effects on soil transport rates and hillslope evolution. *IAHS Publication* **325**: 417–424.

Almond PC, Shanhun FL, Rieser U *et al.* 2007b. An OSL, radiocarbon and tephra isochron-based chronology for Birdlings Flat loess at Ahuriri Quarry, Banks Peninsula, Canterbury, New Zealand. *Quaternary Geochronology* **2**: 4–8.

Almond PC, Tonkin PJ. 1999. Pedogenesis by upbuilding in an extreme leaching and weathering environment, and slow loess accretion, south Westland, New Zealand. *Geoderma* **92**: 1–36.

André M. 1997. Holocene rockwall retreat in Svalbard: a triple-rate evolution. *Earth Surface Processes and Landforms* **22**: 423–440.

Balescu S, Ritz J, Lamothe M *et al.* 2007. Luminescence dating of a gigantic palaeolandslide in the Gobi-Altay mountains, Mongolia. *Quaternary Geochronology* **2**: 290–295.

Becker A, Davenport CA. 2003. Rockfalls triggered by the AD 1356 Basle earthquake. *Terra Nova* **15**: 258–264.

Bell DH, Trangmar BB. 1987. Regolith materials and erosion processes on the Port Hills, Christchurch, New Zealand. *Fifth International Symposium on Landslides*. Lausanne: A.A. Balkema, 93–105.

Berger GW, Tonkin PJ, Pillans BJ. 1996. Thermoluminescence ages of post-glacial loess, Rakaia River, South Island, New Zealand. *Quaternary International* **34–36**: 177–181.

Bertolini G. 2007. Radiocarbon dating on landslides in the Northern Apennines (Italy): landslides and climate Changes,[Q3] 73–80. Q3

Borella J, Quigley M, Vick L. 2016. Anthropocene rockfalls travel farther than prehistoric predecessors. *Science Advances* **2**: e1600969.

Bronk Ramsey C. 2009. Bayesian analysis of radiocarbon dates. *Radiocarbon* **51**: 337–360.

Bull WB, King J, Kong F *et al.* 1994. Lichen dating of coseismic landslide hazards in alpine mountains. *Geomorphology* **10**: 253–264.

Buylaert J, Jain M, Murray AS, *et al.* 2012. A robust feldspar luminescence dating method for Middle and Late Pleistocene sediments. *Boreas* **41**: 435–451.

Chapot MS, Sohbati R, Murray AS *et al.* 2012. Constraining the age of rock art by dating a rockfall event using sediment and rock-surface luminescence dating techniques. *Quaternary Geochronology* **13**: 18–25.

Cordes SE, Stock GM, Schwab BE *et al.* 2013. Supporting evidence for a 9.6 1 ka rock fall originating from Glacier Point in Yosemite Valley, California. *Environmental and Engineering Geoscience* **19**: 345–361.

Fattahi M, Walker R, Hollingsworth J *et al.* 2006. Holocene slip-rate on the Sabzevar thrust fault, NE Iran, determined using optically stimulated luminescence (OSL). *Earth and Planetary Science Letters* **245**: 673–684.

Forsyth PJ, Barrell DJA, Jongens R. 2008. *Geology of the Christchurch Area. 1: 250 000 Geological map 16*. Lower Hutt: Institute of Geological and Nuclear Sciences.

Fuchs M, Fischer M, Reverman R. 2010. Colluvial and alluvial sediment archives temporally resolved by OSL dating: implications for reconstructing soil erosion. *Quaternary Geochronology* **5**: 269–273.

Fuchs M, Lang A. 2009. Luminescence dating of hillslope deposits – a review. *Geomorphology* **109**: 17–26.

Fuchs M, Lang A, Wagner GA. 2004. The history of Holocene soil erosion in the Phlious Basin, NE Peloponnese, Greece, based on optical dating. *Holocene* **14**: 334–345.

Fuller IC, Macklin MG, Richardson JM. 2015. The geography of the Anthropocene in New Zealand: differential river catchment response to human impact. *Geographical Research* **53**: 255–269.

Glade T. 2003. Landslide occurrence as a response to land use change: a review of evidence from New Zealand. *Catena* **51**: 297–314.

Goh KM, Molloy BPJ, Rafter TA. 1977. Radiocarbon dating of Quaternary loess deposits, Banks Peninsula, Canterbury, New Zealand. *Quaternary Research* **7**: 177–196.

Goh KM, Tonkin PJ, Rafter TA. 1978. Implications of improved radiocarbon dates of Timaru peats on Quaternary loess stratigraphy. *New Zealand Journal of Geology and Geophysics* **21**: 463–466.

Grapes R, Rieser U, Wang N. 2010a. Optical luminescence dating of a loess section containing a critical tephra marker horizon, SW North Island of New Zealand. *Quaternary Geochronology* **5**: 164–169.

Grapes R, Rieser U, Wang N. 2010b. Reply to Lowe, D.J., Wilson, C.J.N., Newnham, R.M., Hogg, A.G. comment on Grapes, R., Rieser, U., Wang, N., 2010. Optical luminescence dating of a loess section containing a critical tephra marker horizon, SW North Island of New Zealand. *Quaternary Geochronology* **5**: 497–501.

Griffiths E. 1973. Loess of Banks Peninsula. *New Zealand Journal of Geology and Geophysics* **16**: 657–675.

Hampton SJ, Cole JW. 2009. Lyttelton Volcano, Banks Peninsula, New Zealand: primary volcanic landforms and eruptive centre identification. *Geomorphology* **104**: 284–298.

Hanson P, Mason JA, Goble RJ. 2004. Episodic Late Quaternary slopewash deposition as recorded in colluvial aprons, Southeastern Wyoming. *Quaternary Science Reviews* **23**: 1835–1846.

Harding JS. 2003. Historic deforestation and the fate of endemic invertebrate species in streams. *New Zealand Journal of Marine and Freshwater Research* **37**: 333–345.

Heimsath AM, Chappell J, Spooner NA *et al.* 2002. Creeping soil. *Geology* **30**: 111–114.

Heimsath AM, Dietrich WE, Nishiizumi K *et al.* 2001. Stochastic processes of soil production and transport: erosion rates, topographic variation and cosmogenic nuclides in the Oregon Coast Range. *Earth Surface Processes and Landforms* **26**: 531–552.

Heron D, Lukovic B, Massey C *et al.* 2014. GIS modelling in support of earthquake-induced rockfall and cliff collapse risk assessment in the Port Hills, Christchurch. *Journal of Spatial Science* **59**: 313–332.

Heyman J, Stroeven AP, Harbor JM *et al.* 2011. Too young or too old: evaluating cosmogenic exposure dating based on an analysis of compiled boulder exposure ages. *Earth and Planetary Science Letters* **302**: 71–80.

Hogg A. 2013. SHCal13 Southern Hemisphere calibration, 0–50,000 years cal BP. *Radiocarbon* **55**: 1889–1903.

Hughes MW, Almond PC, Roering JJ *et al.* 2010. Late Quaternary loess landscape evolution on an active tectonic margin, Charwell Basin, South Island, New Zealand. *Geomorphology* **122**: 294–308.

Ives D. 1973. Nature and distribution of loess in Canterbury, New Zealand. *New Zealand Journal of Geology and Geophysics* **16**: 587–610.

Jibson RW. 1996. Use of landslides for paleoseismic analysis. *Engineering Geology* **43**: 291–323.

Johnson DL. 1990. Biomantle evolution and the redistribution of earth materials and artifacts. *Soil Science* **149**: 84–102.

Johnson DL, Domier JEJ, Johnson DN. 2005. Animating the biodynamics of soil thickness using process vector analysis: a dynamic denudation approach to soil formation. *Geomorphology* **67**: 23–46.

Johnson DL, Watson-stegner D. 1987. Evolution model of pedogenesis. *Soil Science* **143**: 349–366.

Johnson DL, Watson-stegner D, Johnson DN *et al.* 1987. Proisotropic and proanisotropic processes of pedoturbation. *Soil Science* **143**: 278–292.

Kanari M. 2008. *Evaluation of rockfall hazard to Qiryat Shemona – Possible correlation to earthquakes*. MSc Thesis, Tel Aviv University, Jerusalem.

Kasai M, Brierley GJ, Page MJ *et al.* 2005. Impacts of land use change on patterns of sediment flux in Weraamaia catchment, New Zealand. *Catena* **64**: 27–60.

Kettner AJ, Gomez B, Syvitski JPM. 2007. Modeling suspended sediment discharge from the Waipaoa River system, New Zealand: the last 3000 years. *Water Resources Research* **43**: W07411.

Khajavi N, Quigley M, McColl S *et al.* 2012. Seismically induced boulder displacement in the Port Hills, New Zealand during the 2010 Darfield (Canterbury) earthquake. *New Zealand Journal of Geology and Geophysics* **55**: 271–278.

Lang A, Moya J, Corominas J *et al.* 1999. Classic and new dating methods for assessing the temporal occurrence of mass movements. *Geomorphology* **30**: 33–52.

Lang A, Wagner GA. 1996. Infrared stimulated luminescence dating of archaeosediments. *Archaeometry* **38**: 129–141.

Luckman BH, Fiske CJ. 1995. Estimating long-term rockfall accretion rates by lichenometry. *Geomorphology*: 233–255.[Q4] Q4

Mackey BH, Quigley MC. 2014. Strong proximal earthquakes revealed by cosmogenic ^{3}He dating of prehistoric rockfalls, Christchurch, New Zealand. *Geology* **42**: 975–978.

Massey CI, McSaveney MJ, Tai T, *et al.* 2014, Determining rockfall risk in Christchurch using rockfalls triggered by the 2010-2011 Canterbury earthquake sequence. *Earthquake Spectra* **30**: 155–181.

Matmon A, Shaked Y, Porat N *et al.* 2005. Landscape development in an hyperarid sandstone environment along the margins of the Dead Sea fault: implications from dated rock falls. *Earth and Planetary Science Letters* **240**: 803–817.

McCarroll D, Shakesby RA, Matthews JA. 2001. Enhanced rockfall activity during the little ice age: further lichenometric evidence from a Norwegian talus. *Permafrost and Periglacial Processes* **12**: 157–164.

McGlone MS. 1989. The Polynesian settlement of New Zealand in relation to environmental and biotic changes. *New Zealand Journal of Ecology* **12**: 115–129.

McWethy DB, Whitlock C, Wilmshurst JM *et al.* 2010. Rapid landscape transformation in South Island, New Zealand, following initial Polynesian settlement. *Proceedings of the National Academy of Sciences of the United States of America* **107**: 21343–21348.

Murray AS, Wintle AG. 2003. The single aliquot regenerative dose protocol: potential for improvements in reliability. *Radiation Measurements* **37**: 377–381.

Rinat Y, Matmon A, Arnold M *et al.* 2014. Holocene rockfalls in the southern Negev Desert, Israel and their relation to Dead Sea fault earthquakes. *Quaternary Research* **81**: 260–273.

Roering JJ, Almond P, Tonkin P *et al.* 2002. Soil transport driven by biological processes over millennial timescales. *Geology* **30**: 1115–1118.

Roering JJ, Almond P, Tonkin P *et al.* 2004. Constraining climatic controls on hillslope dynamics using a coupled model for the transport of soil and tracers: Application to loess-mantled hillslopes, South Island, New Zealand. *Journal of Geophysical Research: Earth Surface* **109**: 1–19.

Rowan AV, Roberts HM, Jones MA *et al.* 2012. Optically stimulated luminescence dating of glaciofluvial sediments on the Canterbury Plains, South Island, New Zealand. *Quaternary Geochronology* **8**: 10–22.

Runge ECA, Goh KM, Rafter TA. 1973. Radiocarbon chronology and problems in the interpretation of Quaternary loess deposits, South Canterbury, New Zealand. *Soil Science Society of America Proceedings* **37**: 742–746.

Shulmeister J, Soons JM, Berger GW *et al.* 1999. Environmental and sea-level changes on Banks Peninsula (Canterbury, New Zealand) through three glaciation–interglaciation cycles. *Palaeogeography Palaeoclimatology Palaeoecology* **152**: 101–127.

Sohbati R, Borella J, Murray AS *et al.* 2016. Optical dating of loessic hillslope sediments constrains timing of prehistoric rockfalls, Christchurch, New Zealand. *Journal of Quaternary Science*.

Soons JM, Moar NT, Shulmeister J *et al.* 2002. Quaternary vegetation and climate changes on Banks Peninsula, South Island, New Zealand. *Global and Planetary Change* **33**: 301–314.

Stock GM, Collins BD. 2014b. Reducing rockfall risk in Yosemite National Park. *Eos, Transactions American Geophysical Union* **95**: 261–263.

Stock GM, Luco N, Collins BD *et al.* 2014a. Quantitative rock-fall hazard and risk assessment for Yosemite Valley, Yosemite National Park, California. *U.S. Geological Survey Scientific Investigations Report 2014-5129*.

Stoffel M. 2006. A review of studies dealing with tree rings and rockfall activity: the role of dendrogeomorphology in natural hazard research. *Natural Hazards* **39**: 51–70.

Stout M, L. 1969. Radiocarbon dating of landslides in southern California and engineering geology implications. *Geological Society of America Special Papers* **123**: 167–180.

Syvitski JP, Vörösmarty CJ, Kettner AJ *et al.* 2005. Impact of humans on the flux of terrestrial sediment to the global coastal ocean. *Science* **308**: 376–380.

Tonkin PJ, Runge ECA, Ives DW. 1974. A study of Late Pleistocene loess deposits, South Canterbury, New Zealand. *Quaternary Research* **4**: 217–231.

Vandergoes MJ, Hogg AG, Lowe DJ *et al.* 2013. A revised age for the Kawakawa/Oruanui tephra, a key marker for the Last Glacial Maximum in New Zealand. *Quaternary Science Reviews* **74**: 195–201.

Wilson HD. 1993. Bioclimatic zones and Banks Peninsula. *Canterbury Botanical Society Journal* **27**: 22–29.

Wilson HD. 2008. *Natural History of Banks Peninsula*. Christchurch: Canterbury University Press.

Wilson HD. 2013. *Plant Life on Banks Peninsula*. Cromwell, New Zealand: Manuka Press.

Woodward CA, Shulmeister J. 2005. A Holocene record of human induced and natural environmental change from Lake Forsyth (Te Wairewa), New Zealand. *Journal of Paleolimnology* **34**: 481–501.

Author Query Form (JQS/2905)

Special Instruction: Author please include responses to queries with your other corrections and return by e-mail.

Q1: Please confirm that given names (red) and surnames/family names (green) have been identified correctly.

Q2: Please check the citation for Hogg et al., 2013. Reference has been provided as Hogg, 2013.

Q3: Bertolini 2007: please confirm journal title/book title/editors/ publisher.

Q4: Luckman & Fiske 1995. Please provide journal volume number

Required software to eAnnotate PDFs: Adobe Acrobat Professional or Acrobat Reader (version 8.0 or above). (Note that this document uses screenshots from Acrobat Reader 9. For screenshots from Acrobat Reader X, a separate document is available on the journal e-proofing site.)
The latest version of Acrobat Reader can be downloaded for free at: http://get.adobe.com/reader/

Once you have Acrobat Reader 8, or higher, open on your PC you should see the Commenting Toolbar:

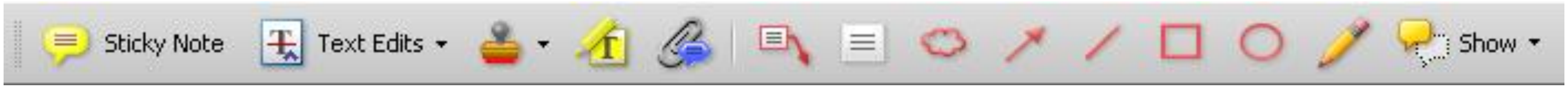

****(If the above toolbar does not appear automatically go to *Tools>Comment & Markup>Show Comment & Markup Toolbar*)****

1. Replacement Text Tool — For replacing text.

Strikes a line through text and opens up a replacement text box.

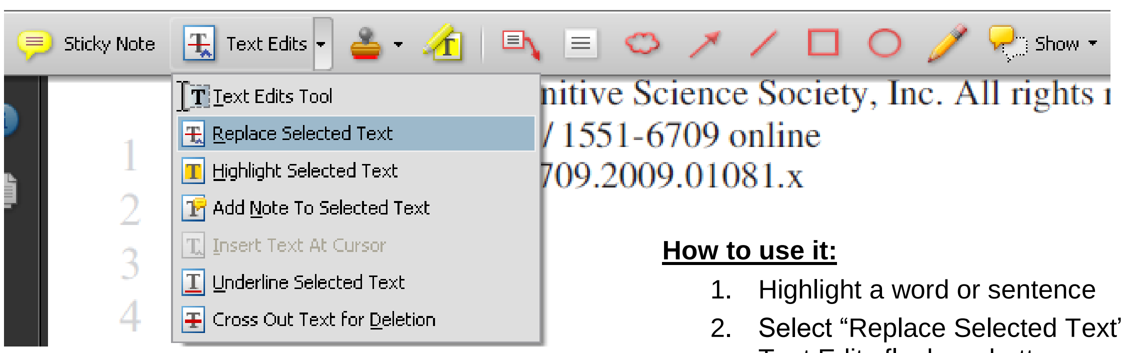

How to use it:

1. Highlight a word or sentence
2. Select "Replace Selected Text" from the Text Edits fly down button
3. Type replacement text in blue box

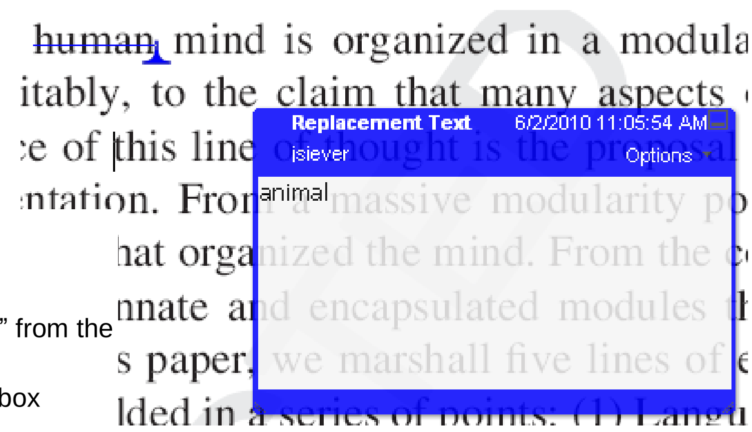

2. Cross-out Text Tool — For deleting text.

Strikes a red line through selected text.

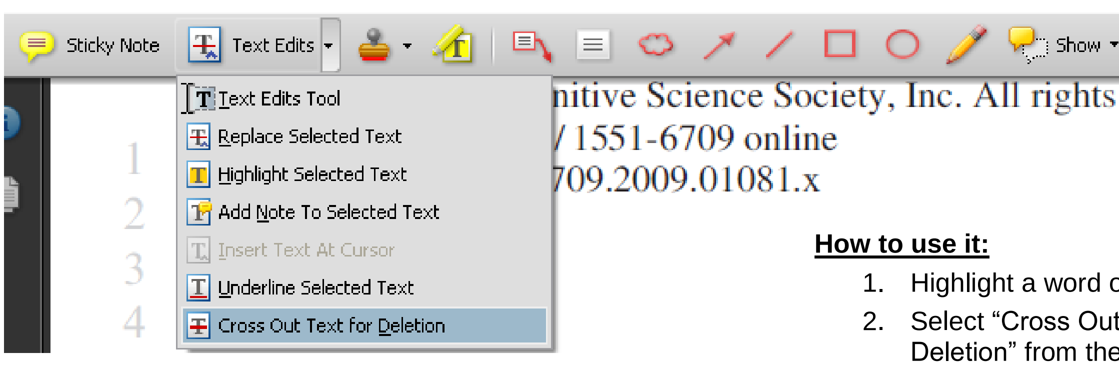

How to use it:

1. Highlight a word or sentence
2. Select "Cross Out Text for Deletion" from the Text Edits fly down button

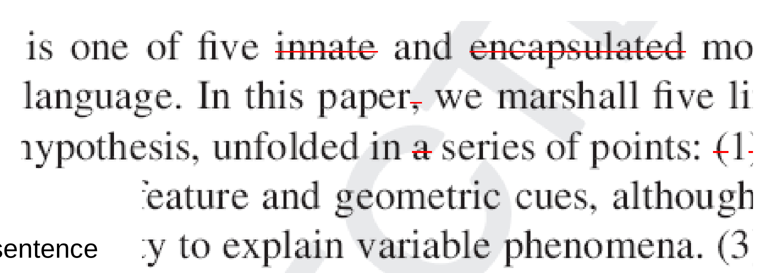

3. Highlight Tool — For highlighting a selection to be changed to bold or italic.

Highlights text in yellow and opens up a text box.

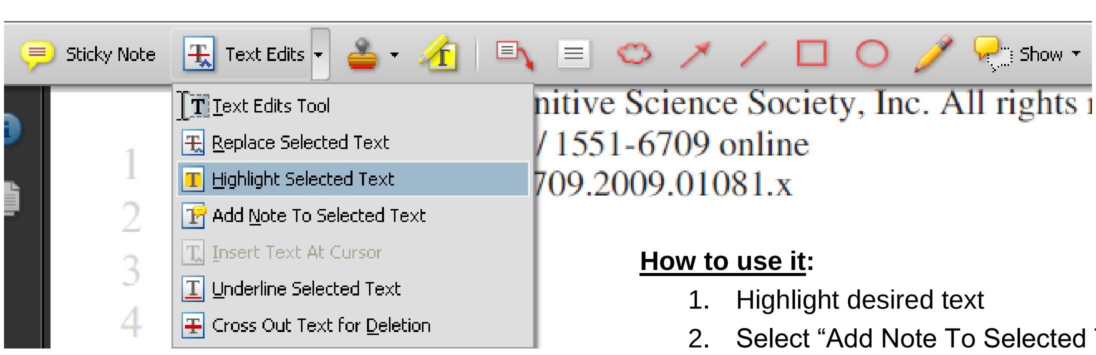

How to use it:

1. Highlight desired text
2. Select "Add Note To Selected Text" from the Text Edits fly down button
3. Type a note detailing required change in the yellow box

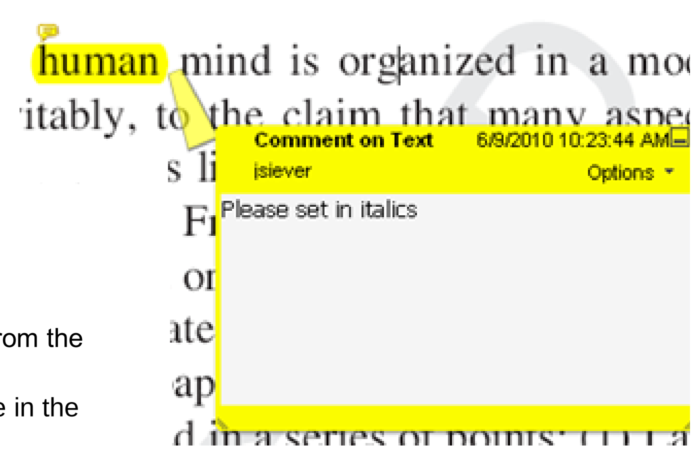

4. Note Tool — For making notes at specific points in the text

Marks a point on the paper where a note or question needs to be addressed.

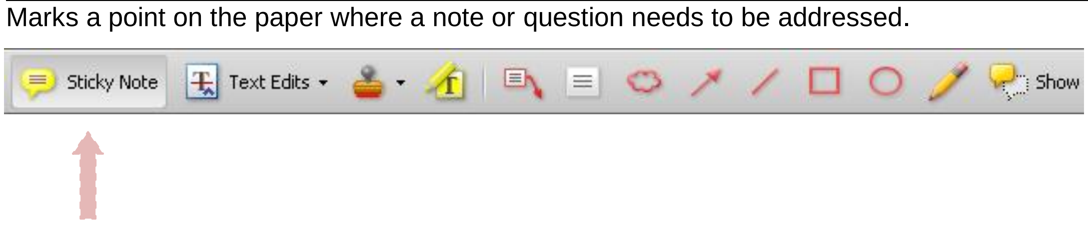

How to use it:

1. Select the Sticky Note icon from the commenting toolbar
2. Click where the yellow speech bubble symbol needs to appear and a yellow text box will appear
3. Type comment into the yellow text box

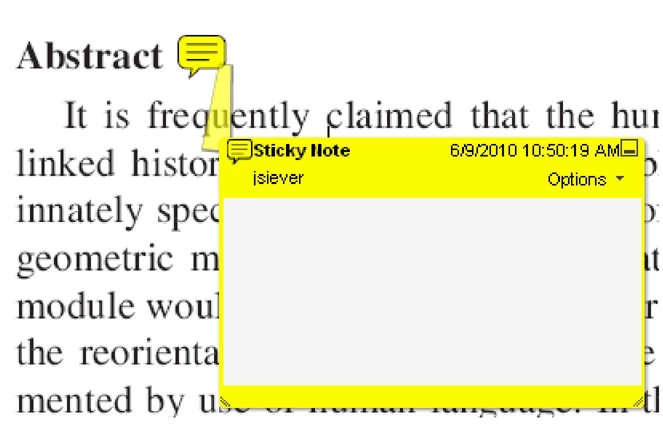

5. Drawing Markup Tools — For circling parts of figures or spaces that require changes

These tools allow you to draw circles, lines and comment on these marks.

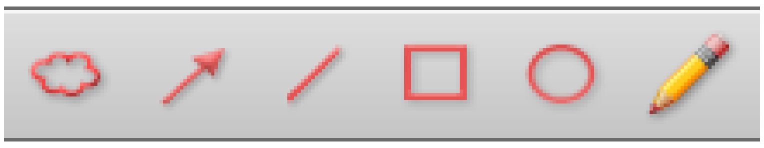

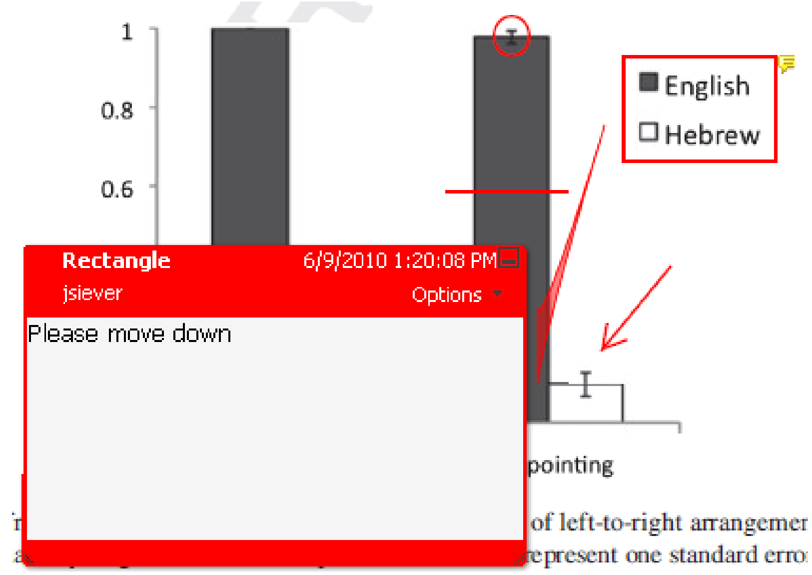

How to use it:

1. Click on one of shape icons in the Commenting Toolbar
2. Draw the selected shape with the cursor
3. Once finished, move the cursor over the shape until an arrowhead appears and double click
4. Type the details of the required change in the red box

6. Attach File Tool — For inserting large amounts of text or replacement figures as a files.

Inserts symbol and speech bubble where a file has been inserted.

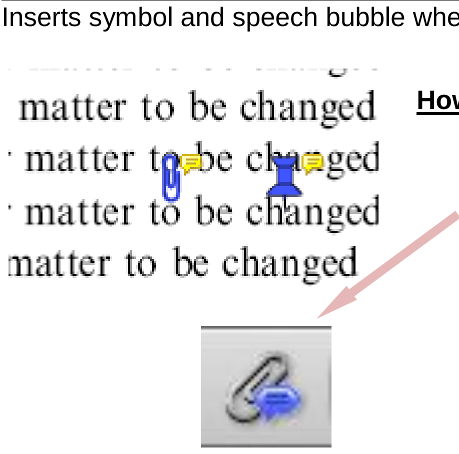

How to use it:

1. Right click on the Commenting Toolbar
2. Select "Attach a File as a Comment"
3. Click on paperclip icon that appears in the Commenting Toolbar
4. Click where you want to insert the attachment
5. Select the saved file from your PC or network
6. Select type of icon to appear (paperclip, graph, attachment or tag) and close

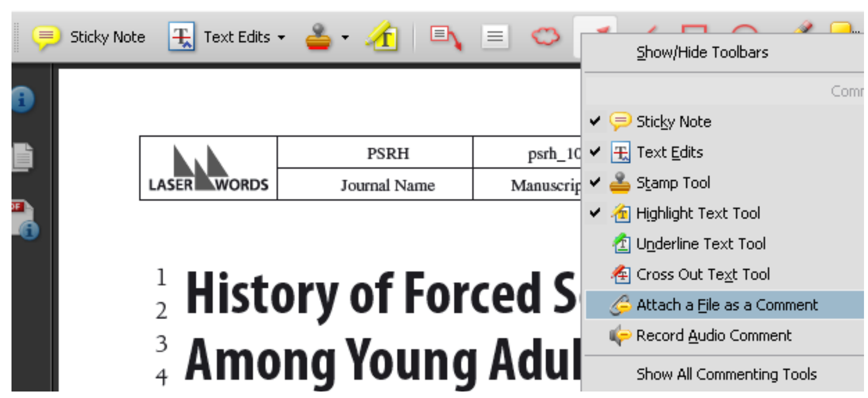

7. Approved Tool (Stamp) — For approving a proof if no corrections are required.

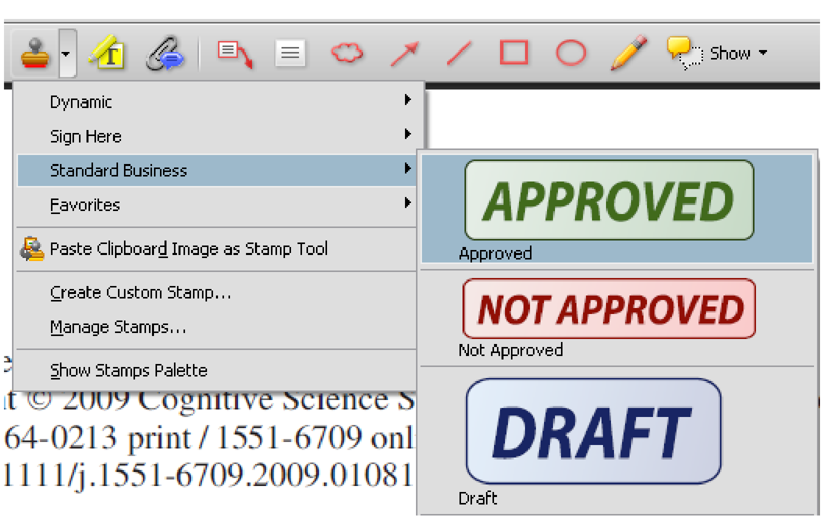

How to use it:

1. Click on the Stamp Tool in the toolbar
2. Select the Approved rubber stamp from the 'standard business' selection
3. Click on the text where you want to rubber stamp to appear (usually first page)

Help

For further information on how to annotate proofs click on the Help button to activate a list of instructions: